Renewable and Sustainable Energy Reviews 37 (2014) 480–501

Contents lists available at ScienceDirect

Renewable and Sustainable Energy Reviews

journal homepage: www.elsevier.com/locate/rser

Indium alloy-sealed vacuum glazing development and context

Yueping Fang [a,*], Trevor J. Hyde [a], Farid Arya [a], Neil Hewitt [a], Philip C. Eames [b], Brian Norton [c], Seth Miller [d]

[a] School of the Built Environment, University of Ulster, BT37 0QB Newtownabbey, Northern Ireland, UK
[b] Centre for Renewable Energy Systems Technology, University of Loughborough, Loughborough, UK
[c] Dublin Energy Lab, Dublin Institute of Technology, Dublin, Ireland
[d] EverSealed Windows, Inc. 1999 Interlocken Drive, Evergreen, CO 80439-8952, USA

ARTICLE INFO

Article history:
Received 19 September 2013
Accepted 11 May 2014
Available online 7 June 2014

Keywords:
Vacuum glazing
Finite element model
Finite volume model
Low-emittance coating
Triple vacuum glazing
Hybrid vacuum glazing
Electrochromic vacuum glazing

ABSTRACT

Vacuum glazing consists of two parallel glass sheets with a narrow vacuum gap in between. The sheets are separated by an array of support pillars under the influence of atmospheric pressure imposed on the external surfaces of the two glass sheets. The vacuum gap sealed by a sealant (either solder glass or indium alloy) minimizes the air heat conduction and convection across the glazing. One or two high performance low emittance (low-e) coatings deposited on the internal surface(s) within the vacuum gap reduces the radiative heat transfer to a very low level. The heat transmittance of 0.80 W m^{-2} K^{-1} and 0.86 W m^{-2} K^{-1} at the central area of vacuum glazing with two low-e coatings and support pillars of 0.25 mm and 0.4 mm in diameter were achieved and experimentally characterized using the guarded hot box calorimeters by the University of Sydney and the University of Ulster, respectively. If combined with solar control glazing such as electrochromic (EC) glazing, it has a great potential to significantly reduce the load of heating in winter and cooling in summer and to provide thermal comfort for the occupants. If combined with the third glass sheet forming a gas filled or second vacuum gap, the heat transmittance will be further reduced. In this work, the basic characteristics and fabrication process of vacuum glazing are reviewed. The potential performance of vacuum glazing, EC vacuum glazing and other hybrid vacuum glazing with second either gas filled gap or vacuum gap are presented.

Contents

* Corresponding author. Tel.: +44 2890366808; fax: +44 2890368239.
E-mail addresses: fangyueping@hotmail.com, y.fang@ulster.ac.uk (Y. Fang).

http://dx.doi.org/10.1016/j.rser.2014.05.029
1364-0321/

1. Introduction

Among all building fabric components, usually windows exhibit the worst thermal performance since they employ glass panes to allow sunlight to get in and occupants to view the outside. Vacuum glazing comprises two sheets of glass coated with low-e coatings, separated by arrays of support pillars to counteract atmospheric pressure. Heat loss through the windows occurs in three ways: conduction, convection and radiation. The low-e coatings reduce radiative heat loss to a very low level and the vacuum space (<0.1 Pa) between the two glass sheets eliminates heat conduction and convection. The thermal transmittance, *U*-value, of vacuum glazing is one third of that of a typical gas filled double glazing.

Vacuum glazing was first proposed by Zoller in 1913 with a patent granted in 1924 [1]. Since 1913, many patents [2–22] have been published on this topic. Only recently successful fabrication of vacuum glazing has been reported [23–27]. In the 1980s, Benson and his group at the National Renewable Energy Laboratory in Colorado, U.S.A. published two conference papers [28,29], a patent [14], and a series of reports [28–30]. However, this group did not succeed in fabricating a durable vacuum glazing with good thermal performance. Benson's group used a laser to fuse two sheets of glass together within a vacuum chamber to form a periphery edge seal for the vacuum gap. Although the edge seal was formed successfully, the vacuum level achieved was not low enough to achieve a thermal transmittance less than 1.0 W m^{-2} K^{-1}. The first reported successful production of vacuum glazing was in 1989 from the University of Sydney (USD) [31]. Since that time, many samples of vacuum glazing with an air-to-air, center-of-glazing thermal transmittance *U*-value of 0.8 W m^{-2} K^{-1} have been produced at the USD using a solder glass edge sealing technique [32]. This system has been commercialized by Nippon Sheet Glass Co. Ltd. in Japan under the brand name of "SPACIA". More recently a Chinese company Beijing Synergy Vacuum Glass Technology Co., Ltd. has commercialized vacuum glazing using different types' solder glass, but no formal paper was seen on an academic journal yet.

A different fabrication method of vacuum glazing using a indium alloy edge seal technique was developed at the University of Ulster (UU); vacuum glazing samples incorporating two *K*-glass [33] sheets were produced with the center-of-glazing *U*-value of 0.86 W m^{-2} K^{-1}, and significant work done on different aspects of vacuum glazing including thermal characterization, thermal ageing tests, thermal behaviour modelling [24–27,34–43].

The key difference between the two fabrication methods developed by the Sydney and the Ulster group is the sealing techniques used to join the two glass panes. The Sydney group use solder glass (melting point of about 450 °C) to seal the vacuum gap which has been proved to work well. But at temperatures of about 450 °C, many soft low-e coatings and tempered glass will be degraded. Nowadays in many jurisdictions for a range of contexts, it is mandatory to use tempered glass in buildings; additionally due to its high mechanical strength, using tempered glass in vacuum glazing makes it possible to increase the pillar separation which leads to a reduction in the heat conduction through the pillar array. The Ulster group has successfully fabricated vacuum glazing samples using indium alloy as a sealant, the process developed is carried out at a low temperature (less than 200 °C). Since a variety of soft low-e coatings and tempered glass can withstand these temperatures (less than 200 °C), the indium alloy based sealing technique has an advantage over the solder glass technique in terms of achievable performance.

Significant theoretical and experiment research into the design and performance of low temperature sealed vacuum glazing was performed by the Ulster group. The Ulster group also developed a finite volume model to calculate the thermal performance of vacuum glazing with various frames, low-e coatings, glazing size, glass thickness and solar insolation [34–42] and the predictions were experimentally validated [39–42]. Optimization of vacuum glazing design was theoretically and experimentally undertaken. A guarded hot box calorimeter was developed to characterize the thermal performance of vacuum glazing. A method for estimating the vacuum level was developed by comparing the measured and simulated glass temperature profiles [35,45]

Within recent 10 years, the companies Guardian, EverSealed Window Inc., and a German group Grenzebach GmbH tried to use either a strip of metal or very thin stainless steel foil as flexible edge seal using ultrasonic bonding to adapt the extreme weather. The stress at the edge area of glass panes caused by the bonding between the flexible edge seal and glass panes is much smaller than that when using either solder glass or indium alloy edge seal. However no successful samples were reported yet to date.

2. Construction and fabrication of a functioning vacuum glazing

Fig. 2.1 shows a schematic diagram of the vacuum glazing developed at the USD. The vacuum glazing was made of two sheets of soda lime glass with a thickness of 3 or 4 mm. The inner surface of one or both sheets may be coated with a transparent low-e coating. Pyrolitically deposited "hard" coatings include

Nomenclature

A	area of test sample (m^2)
B	molar gas constant
b	width of glazing (m)
c	height of glazing (m)
a	radius of support pillar (m)
d	separation of two parallel glass panes (m)
E	black body radiation function
h	surface heat transfer coefficient ($W\,m^{-2}\,K^{-1}$)
k	thermal conductivity ($W\,m^{-1}\,K^{-1}$)
l	characteristic distance
M	molar mass of gas
P	pressure (Pa)
Q	heat transfer (W)
R	thermal resistance associated with heat flow per m^2 ($m^2\,W\ K^{-1}$)
s	pillar separation (m)
t	glass thickness (m)
T	temperature (°C)
U	thermal transmission ($W\,m^{-2}\,K^{-1}$)
w	frame rebate depth (m)

Greek letters

α	molar combined accommodation coefficient
ν	solar absorption
λ	wavelength (nm)
γ	specific heat ratio of the gas
θ	radiation direction angle between the beam irradiation and the normal to the surface
τ	solar direct transmittance
ρ	solar reflectance
φ	total solar radiation ($W\,m^{-2}$)
ε	hemispheric emittance of a surface
Δ	difference
σ	Stefan-Boltzmann constant ($5.67\times10^{-8}\,W\,m^{-2}\,K^{-4}$)

Subscripts

1, 2	refer to vacuum gaps 1 and 2
a–a	refer to air to air
i, o	refer to warm and cold ambient temperatures
j, k	refer to the glass surfaces
g	glass
m	glass pane number of the TVG
n	vacuum gap number
s	support pillar
r	radiation
w	window

K glass [33], Energy Advantage (Libby Owens Ford), Sungate 500 (PPG), Comfort EM 5000 (Glaverbel) and Comfort E^2 (AFG Industries) [32]. The edge seal was made with solder glass which is a low melting point glass with a thermal expansion coefficient matching that of the glass sheets. When forming the solder glass edge seal, the entire structure was heated to about 500 °C for 1 h, and then cooled slowly to room temperature. To date only hard low-e coatings of tin oxide have been found to survive the manufacture process without degradation. The support pillars fabricated to date at the USD were made of Inconel 718, which is a high strength, heat resistant, nickel-based alloy; they were typically about 0.25 mm in diameter and 0.15 mm height [32].

The fabrication process is shown in Table 2.1 [49]:

The structure of the vacuum glazing fabricated by the UU is illustrated in Fig. 2.2. The edge seal was made of indium alloy. Two fabrication methods were developed. The first one is called of vacuum chamber method [26]; the second one is called of pump-out method [27].

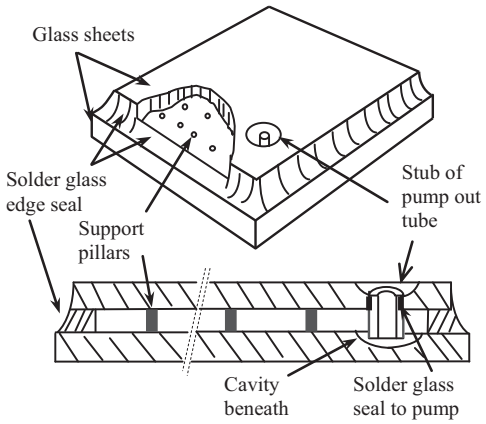

Fig. 2.1. Schematic diagram of vacuum glazing, fabricated at USD [32].

Vacuum chamber method: This is a one stage method; both "edge seal formation" and subsequent "pumping-out" processes are completed simultaneously within a vacuum chamber as shown in Fig. 2.3. Four 1000 W infrared lamps are employed as the heat sources to melt the indium alloy.

The detailed fabrication processes of the vacuum chamber method are shown in Table 2.2:

Pump out method: The pump-out method is a two stage method; the setup of such a system is shown in Fig. 2.4. At the first stage the edge seal is formed in a vacuum chamber. At the second stage, a high vacuum is created between the glass panes using a turbo-molecular pump; this process is completed in a conventional oven. The detailed processes are listed in Table 2.3:

The main difference between vacuum glazing samples fabricated using the UU and the USD methods:

- The USD method uses solder glass as a sealant with melting point of 450–530 °C. The UU uses indium alloy as a sealant with melting point of around 156 °C.
- In the USD method, the upper glass pane is slightly smaller than the lower one as shown in Fig. 2.1 to facilitate the setting of solder glass paste to seal the vacuum gap; in the UU method, the size of the two glass panes are the same as shown in Figs. 2.2 and 2.4.

3. Characteristics of vacuum glazing components

A successful vacuum glazing has:

- a hermitic leak free seal around the edges of the two glass sheets,

Table 2.1
Details of solder glass edge sealing method.

1. The panes are cut to the required size, drill a hole in one of them near a corner to connect the evacuation tube
2. The glass edges are treated to reduce the possibility of breakage and then clean the glass sheets and dry them
3. The pillars are set on the lower glass sheet, the pump-out tube is inserted in the hole drilled in the upper glass sheet
4. Solder glass paste is applied around the pump-out tube, to provide a hermetic seal after melting
5. The upper glass sheet is placed and centred on the support pillars placed on the lower glass sheet. The upper glass sheet is slightly smaller than the lower glass sheet
6. Solder glass paste is applied around the edge of an assembled glazing and then the glazing placed into the oven
7. The entire assembly is heated up to a temperature of around 450 °C at which the solder glass melts, wets the surfaces of the glass sheets, flows by capillary action into the space between them, and forms the hermetic seal around the edges
8. Let the glazing cool to room temperature. The assembly is then evacuated. During the evacuation process, the assembly is heated up in order to outgas the internal surfaces. This outgassing is performed at relatively low temperatures, typically between 100 °C and 250 °C. The evacuation and bake-out process takes about 2 to 4 h
9. The assembly is let cool to room temperature and the end of the pump out tube is melted, and sealed. This melting process is accomplished by positioning a heating tungsten coil close to the pump out tube

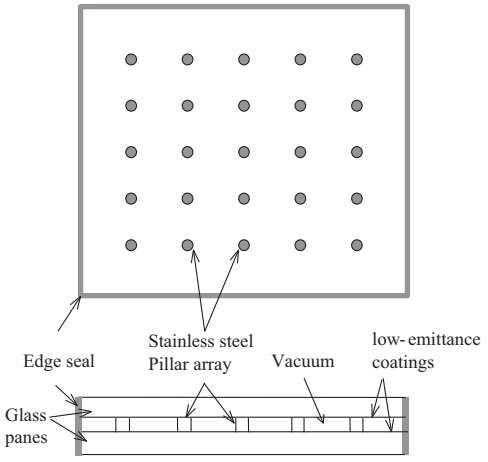

Fig. 2.2. A schematic diagram of a vacuum glazing fabricated using the vacuum chamber.

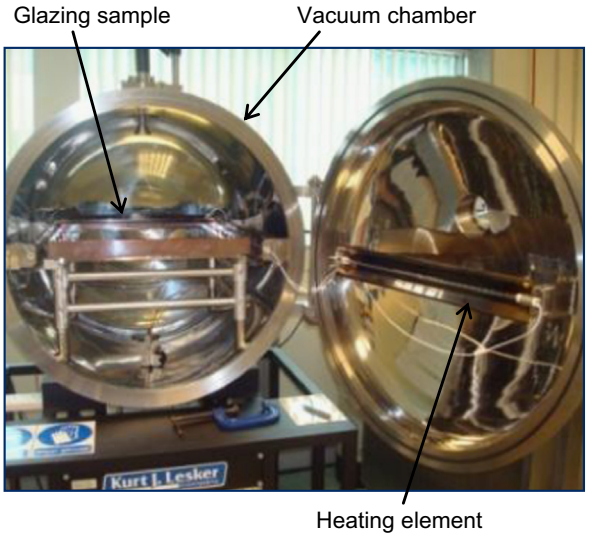

Fig. 2.3. Vacuum chamber for fabricating vacuum glazing.

- a stable vacuum (< 0.1 Pa) [50] in the space between the sheets,
- internal transparent low-e coatings which reduce radiative heat transfer between the sheets to a very low level,
- an array of mechanical support pillars which maintain the separation of the glass sheets under atmospheric pressure,
- sufficiently low tensile stresses due to atmospheric pressure and temperature difference (maximum external tensile stress above the pillars is less than 4 MPa) that the probability of mechanical failure of the device is tolerably small (less than 0.008) over its service life [32].

Fig. 3.1 shows the heat transfer processes within a vacuum glazing. The detailed thermal performance analysis for each part of vacuum glazing is presented in the following sections.

3.1. Edge seal

3.1.1. Edge seal techniques

To form the edge seal in the vacuum glazing produced by the Sydney group solder glass is used with a melting point of about 450–530 °C which is much lower than the softening temperature of the float glass pane. The thermal expansion coefficient of the solder glass is similar to that of the glass panes so that the structure contains very little stress upon completion of the fusing operation. The drawback of solder glass is that its melting temperature is too high (about 450 °C) to be used in conjunction with many soft low-e coatings and tempered glass. To date only tin oxide has been found to be able to withstand this temperature without severe degradation. Low temperature melting solder glass also has insufficient long-term durability to moisture ingress [24]. The Ulster team successfully fabricated vacuum glazing using indium alloy as a sealant [26,27]. Although indium alloy and soda lime glass panes have different thermal expansion coefficients, glass breakage was not observed during thermal cycling. Indium alloy has a low vapour pressure at ambient temperatures therefore it can be used in vacuum glazing without contributing to vacuum pressure increase. Compressing indium alloy wire between two glass panes forms an impermeable vacuum seal which, although physically weak, can be augmented by an adhesive to provide the required strength characteristics. Since the melting point of indium alloy is around 156 °C, almost all kinds of low-e coatings and tempered glass can tolerate this temperature, therefore they can be used in the construction of indium alloy based vacuum glazing [24].

Although the thermal conductivity of solder glass (1 W m^{-1} K^{-1}) and indium alloy (83.7 W m^{-1} K^{-1}) are very different, the difference in *U*-value of solder glass and indium alloy based vacuum glazing is very small if an appropriate framing system is used. The thermal performance of a vacuum glazing with 3 mm and 6 mm wide edge seal were simulated under ASTM winter conditions, and the results are presented in Table 3.1 [45]. The frame rebates w_1 and w_2 were 10 mm. The emittance of the low-e coatings was 0.18.

Table 3.1 shows that the difference in heat conductance (*C*-value) and *U*-value of indium alloy and solder glass based vacuum glazing is less than 0.005 W m^{-2} K^{-1}. With the proper frame insulation, the thermal performance of a vacuum glazing with an indium alloy edge seal will be similar to that of a vacuum glazing with a solder glass edge seal. A new technique by which a metal is directly bonded to glass panes in a vacuum glazing structure to form the edge seal, has been reported [51], and a *U*-value of 0.6 W m^{-2} K^{-1} is expected; however this has not been

Table 2.2
Details of the vacuum chamber method of fabrication of indium alloy based vacuum glazing.

1. The glass panes are cut to size, cleaned using acetone and then de-ionised water; baked out in a conventional oven at 200 °C
2. A thin layer of indium alloy with a width of 6 mm is applied along the periphery of the two glass sheets using an ultrasonic soldering iron
3. The pillars with a diameter of 0.3 mm and height of 0.15 mm are spaced at 25 mm intervals using a vacuum wand on a regular square grid on the lower glass pane
4. The upper glass sheet is set on the lower one so that the indium alloy layers on both panes are aligned
5. The assembly is put into a vacuum chamber which is then evacuated to 10^{-5} Pa. The vacuum chamber temperature is increased up to 150 °C for outgassing purpose for 10 h, and then the temperature is increased up to 170 °C to melt the indium alloy layer to form the edge seal
6. The heating system is switched off and the sample is let cool down overnight to room temperature
7. The vacuum pump is switched off, the chamber is purged with pure nitrogen before moving the sample out

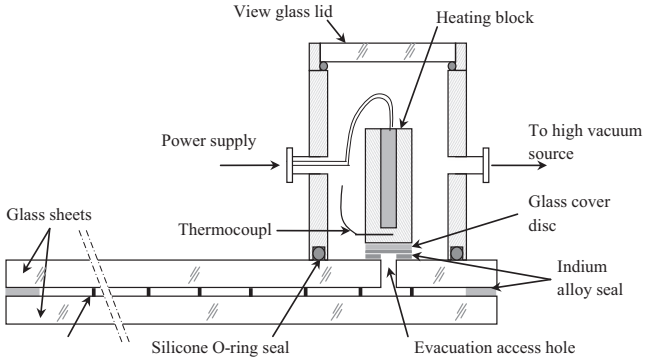

Fig. 2.4. A schematic diagram of the pump-out device [27].

achieved yet. Similarly another metal-to-glass bonding method has been proposed to be used in vacuum glazing [52], again practical sample has not been fabricated yet.

3.1.2. Heat conduction through the edge seal

In vacuum glazing the edge seal acts as a heat short circuit between the glass sheets. Heat flows from the glass sheet on the warm side through the edge seal to the sheet on the cold side; not only does it decrease the overall thermal performance of the glazing, but also it causes temperature variation and stress in the edge region which might result in glazing failure.

Finite element models have been used to predict the *U*-value of different vacuum glazing constructions with different frames, recessed edges and flush insulation structures [53,45]. Using a finite-volume model, the effect of the indium alloy edge seal width and the frame insulation on the heat transfer through indium alloy based vacuum glazing has been simulated and experimentally validated [24,34,35]. The result was similar to that obtained by the Sydney team [32].

An analytical model was developed by the USD [55] to simulate a solder glass based vacuum glazing. Each sheet has a thickness of t, and width of L. The ambient temperatures are T_i and T_0 on the warm and cold sides, with corresponding heat transfer coefficients of h_i and h_0, *respectively*. The glass surfaces near the edge seals are insulated over some distance w_1 and w_2 along the warm and cold sides, respectively [55]. The edge conduction per unit length of edge is proportional to the air to air temperature difference divided by the sum of the glass thermal resistance on both sides of the glazing:

$$Q_{\text{edge}} = \frac{k_{\text{glass}} t (T_i - T_0)}{w_1 + w_2 + \sqrt{k_{\text{glass}} t / h_i} + \sqrt{k_{\text{glass}} t / h_0}} \tag{3.1}$$

The temperature at the inner edge of the seal is:

$$T_{\text{edge}} = \frac{\sqrt{h_i} T_i + \sqrt{h_0} T_0}{\sqrt{h_i} + \sqrt{h_0}} \tag{3.2}$$

In this simple case, the temperature approaches its centre-of-glass value exponentially with a characteristic distance of:

$$l = \sqrt{\frac{k_{\text{glass}} t}{h}} \tag{3.3}$$

where h is the heat transfer coefficient for the side being considered (i.e. h_i, h_0) [53].

The measured temperature profile of the glazing surfaces were in very good agreement with those calculated by analytical and finite element models [35]. Infrared thermo graphic tests were performed on the samples of vacuum glazing by the Sydney [55] and Ulster teams [35]. The error limit of the infrared camera used was ± 0.5 °C [35] as shown in Fig. 3.2.

3.2. Low-e coatings

3.2.1. Glass transmittance and coating properties

The aim of solar control films and glazing is to optimise the thermal and optical performance of windows to provide a comfortable environment within buildings. The solar irradiation (φ_e) incident on a glass surface can be transmitted through, absorbed by or reflected away from the glazing which are referred as $\tau_e\varphi_e$, $\nu_e\varphi_e$ and $\rho_e\varphi_e$, respectively. These three fractions are a function of wavelength λ for different glass samples. For clear window glass, the visible light (0.38–0.78 μm) is transmitted with high transmission, the ultraviolet radiation (0.28–0.38 μm) and the infrared radiation (2 μm and above) are attenuated. At a specific wavelength λ, the measured transmittance τ_λ is known as the monochromatic spectral transmittance. For the full spectrum of the incident solar radiation φ_e, the transmittance is calculated by [56]:

$$\tau_e = \frac{\int_0^\infty \tau_\lambda(\lambda)\varphi_\lambda(\lambda)d\lambda}{\int_0^\infty \varphi_\lambda(\lambda)d\lambda} \tag{3.4}$$

Similar equations can be derived for the absorption α_e, and reflectance ρ_e from the integration of the monochromatic properties across the full electromagnetic spectrum.

In accordance with their different characteristics, thin films on the glazing surface are divided into absorptive, reflective and insulating films. To achieve the lowest *U*-value for vacuum glazing, only insulating films i.e. low-e coatings are considered. Low-e coatings work as a "radiation filter" by reflecting the thermal radiation while remaining transparent to daylight [57]. Within the incoming solar radiation, half of its energy lies in the visible region; the glass with low-e coating transmits solar energy at wavelengths between 0.3 and 2.5 μm very well, it becomes substantially opaque at wavelengths longer than approximately 3 μm which includes nearly all long-wavelength radiation emitted at the characteristic temperatures of internal building surfaces [58]. The glass absorbs internal re-radiated long-wave radiation. This absorbed energy is radiated and transferred to the internal and external environment [59]. The glass with low-e coating acts as a selective reflector, solar transmission is still quite high (about 84% of uncoated glass) but solar reflectance is low (about 16%); the

Table 2.3
Details of the pump out method of fabrication of indium alloy based vacuum glazing.

1. The pump-out hole is drilled near a corner of the upper glass pane, the glass panes are cleaned using acetone, an ultrasonic bath and de-ionised water
2. A thin layer of indium alloy with a width of 6 mm is applied along the periphery of the two glass sheets using an ultrasonic soldering iron
3. The pillars with a diameter of 0.3 mm and height of 0.15 mm are spaced at 25 mm intervals using a vacuum wand on a regular square grid on the lower glass pane. The upper glass sheet is set on the lower one so that the indium alloy layers on both panes are aligned
4. The assembly is put into the vacuum chamber which is then evacuated to 10^{-5} Pa. The vacuum chamber temperature is increased up to 150 °C in about 2 h, and then the temperature is again increased up to 170 °C to melt the indium alloy layer to form the edge seal
5. The heating system is switched off and the sample is let cool down overnight to room temperature
6. The pump-out system is employed as shown in Fig. 2.4, and the evacuation is started to create a vacuum of less than 10^{-5} Pa
7. The pump-out hole is sealed using the heating block provided inside the pump-out device

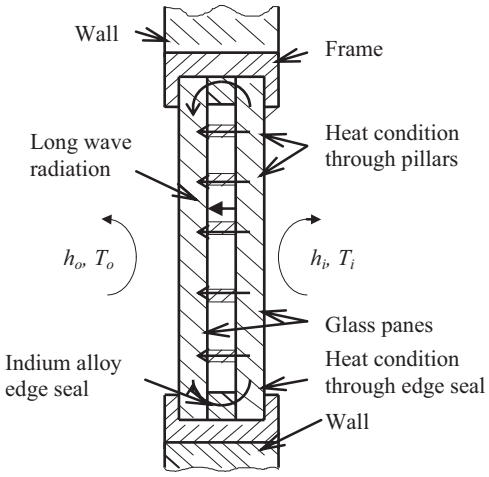

Fig. 3.1. Heat transfer processes in a vacuum glazing.

Table 3.1
The effect of edge seal material characteristics on the thermal performance of a vacuum glazing [45].

MATERIAL	T_1 (°C)	T_2 (°C)	C_{centre} W m^{-2} K^{-1}	C_{total} W m^{-2} K^{-1}	U_{total} W m^{-2} K^{-1}
	Width of edge seal: 3 mm				
Indium alloy	15.59	−16.27	1.437	1.281	1.070
Solder glass	15.60	−16.27	1.433	1.277	1.068
	Width of edge seal: 6 mm				
Indium alloy	15.27	−16.18	1.540	1.372	1.133
Solder glass	15.28	−16.18	1.536	1.369	1.131

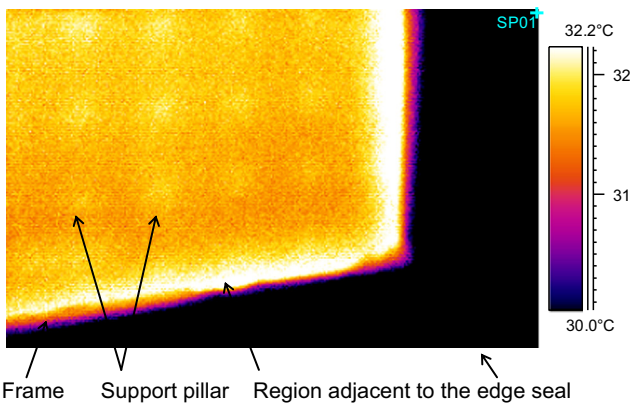

Fig. 3.2. Infrared image of the corner region of a vacuum glazing sample [35].

reflectance is high for the far-infrared wavelengths while the transmission goes to zero.

Tin oxide is a transparent semiconductor. Unlike some other films which require three or four multiple layers of ultra-thin material, transparent semiconductor films can be made in a single, relatively thick layer (about 4–8 millionths of a metre thick). This avoids the quality control issues associated with thin films. Certain highly doped members of this class exhibit high IR reflectance due to their controlled concentration of charge carriers (a material cannot reflect unless it conducts electricity, i.e. carries charge) [57]. Other transparent semiconductors, such as indium oxide, cadmium tin oxide, and indium tin oxide for example might be suitable for low temperature fabrication of vacuum glazing.

The sandwich coatings ZnS/Ag/ZnS suitable for the vacuum glazing fabricated at low temperatures were investigated by a team at the University of Patras [60,61]. The most economical physical vapour deposition method was employed to produce the coatings. It was found that ZnS film has a high refractive index, easy deposition process and low cost, and its thickness was found not to affect the hemispheric emittance. Ag film has a low energy absorption in the visible spectrum. The luminous transmittance of these sandwich coatings is 83.9%, the reflectance to infrared radiation is above 90% and total hemispherical emittance is reduced to 0.03 [60,62] when the thickness of the Ag film is approximately 40 nm. The emittance closely depends on the thickness of the Ag film. It is practical to assume the emittance of low-e coatings within the vacuum gap can be down to 0.03, although in most cases the *K*-glass is used with emittance of 0.16 to 0.18.

3.2.2. *Radiative heat transfer between the two interior glass surfaces*

The radiative heat transfer between the internal glass surfaces depends mainly on the infrared optical properties of these surfaces. To a good approximation, the radiative heat flow can be determined from the classical radiative heat transfer equation [53]:

$$Q_{radiation} = \varepsilon_{effective}\sigma A(T_1^4 - T_2^4) \tag{3.5}$$

where $\varepsilon_{effective}$ is the effective emittance, usually calculated from the hemispherical emittances, ε_1 and ε_2:

$$\varepsilon_{effective} = [\varepsilon_1^{-1} + \varepsilon_2^{-1} - 1]^{-1} \tag{3.6}$$

Eq. (3.6) is only valid for the surface for which the reflectance is independent of the wavelength and the angle of incidence θ (angle between the beam irradiation and the normal to the surface). There is no such ideal surface existing. One method to solve this problem is to define a directional total emittance $\varepsilon(\theta)$ so the hemispherical emittance $\varepsilon_{hemispherical}$ can be written as [63]:

$$\varepsilon_{hemispherical} = \int_0^{\pi/2} e(\theta)\sin\ 2\theta d\theta. \tag{3.7}$$

In this approach, the net rate of radiative heat transfer is given by Eq. (3.8), with:

$$\varepsilon_{\text{effective}} = \int_0^{\pi/2} \frac{\sin 2\theta}{(1/e_1(\theta))+(1/e_2(\theta))-1} d\theta \tag{3.8}$$

This method was justified on the basis that the angular dependence of the reflectance of the most practical surfaces was more significant than their wavelength dependence. For "grey" surfaces, where the reflectance was independent of the wavelength, Eq. (3.8) was correct. For many combinations of surfaces relevant to vacuum glazing, it was not correct. The errors resulting from using either Eqs. (3.6) or (3.8) were typically about 4% for radiative heat transfer between two glass surfaces [63].

For spectral surfaces having reflectance which depend on both wavelength and angle, the net radiative heat transfer can be calculated by integrating over wavelength λ and angle θ [63]:

$$Q_{\text{radiation}} = \int_0^{\pi/2} \sin 2\theta d\theta \int_0^{\infty} \frac{E(\lambda,T_1)-E(\lambda,T_2)}{(1/\varepsilon_1(\lambda,\theta,T_1))+(1/\varepsilon_2(\lambda,\theta,T_2))-1} d\lambda \tag{3.9}$$

In this equation, $\varepsilon(\lambda, \theta, T)$ is the directional spectral emittance of either surface, at temperature T, and $E(\lambda, T)$ is the black body radiation function at temperature T. As will be seen, Eq. (3.9) gives temperature dependence for $Q_{radiation}$ which departs slightly from the $T_1^4 - T_2^4$ dependence predicted by Eq. (3.5).

For transparent low-e coatings, the situation is much more complicated. In the absence of a suitable optical model, the only approach is to make detailed experimental measurements of their optical properties. Zhang et al. [63] therefore developed a free-electron (Drude) model that accurately described the infrared optical properties of pyrolytic transparent low-e coatings such as Pilkington *K* glass [33]. Measurements of near-normal reflectance of *K* glass for wavelengths between 3 μm and 17 μm were used to obtain the three parameters of the Drude model. The three parameters were ζ_∞, ω_p and ω_β. ζ_∞ was the low frequency contribution from the high frequency interband transitions, ω_p was the plasma frequency and ω_β was the damping frequency [64]. The full wavelength and angular dependence of the reflectance of the surface can then be determined using these three parameters. Excellent agreement was obtained between results from these calculations and accurate experimental infrared reflectance data over all angles and wavelengths of interest for this work [63].

If the surface emittance is not strongly dependent on the wavelength, Eq. (3.9) can be approximated to Eq. (3.5), and Eq. (3.8) can be approximated to Eq. (3.6). When the temperatures of the two internal surfaces are not too different, Eq. (3.5) can be linearised by a Taylor series expansion to give the following approximation for the radiative conductance:

$$Q_{\text{radiation}} = \varepsilon_{\text{effective}} \sigma A (T_1^4 - T_2^4) = 4\varepsilon_{\text{effective}} \sigma A T_m^3 \Delta T \tag{3.10}$$

$$C_{\text{radiation}} = 4\varepsilon_{\text{effective}} \sigma T^3 \tag{3.11}$$

where $T_m = (T_1 + T_2)/2$, and $\Delta T = T_1 - T_2$, T_1 and T_2 are the average surface temperatures on the interior and exterior glass surfaces, respectively.

The predicted heat transmission *U*-value of the total window and the centre-of-glass area with boundaries of 63.5 mm from each sightline [65], in which the edge effect has a little influence, were calculated and are presented in Fig. 3.3. It can be seen that with increasing low-e coating emittance, the *U*-value of both the total window and the centre-of-glass area increase. The *U*-value of a vacuum glazing with two low-e coatings is lower than that with one low-e coating and one non-coated float glass pane (emittance value: 0.87), however when the emittance of the low-e coating is close to 0.02, the use of two low-e coatings rather than one gives limited reduction in the *U*-values of vacuum glazing. The use of a single low-e coating in a vacuum glazing can provide acceptable performance.

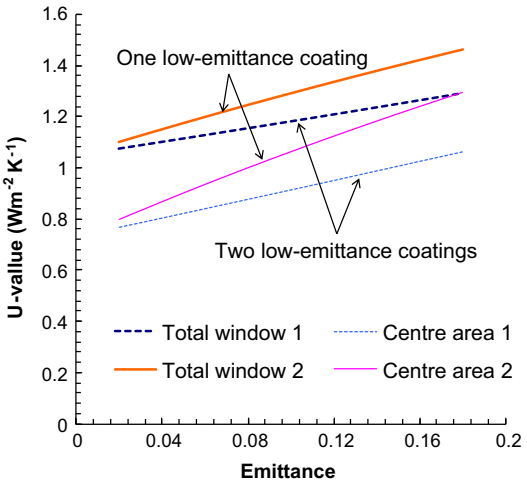

Fig. 3.3. *U*-values of vacuum glazing with various emittance values and one or two low-e coatings [42].

Table 3.2
Comparison between predicted and experimentally determined overall heat transfer coefficients for vacuum glazing with different low-e coatings. In vacuum glazing A: $\varepsilon_1 = 0.16$, $\varepsilon_2 = 0.16$; vacuum glazing B: $\varepsilon_1 = 0.12$, $\varepsilon_2 = 0.16$; vacuum glazing C: $\varepsilon_1 = 0.04$, $\varepsilon_2 = 0.16$.

Vacuum glazing sample no.	Heat transmission ($W\,m^{-2}\,K^{-1}$)			
	Predicted		Experimentally determined	
	U_{centre}	U_W	U_{centre}	U_W
A	1.06	1.29	1.07 ± 0.09	1.30 ± 0.11
B	0.97	1.22	1.00 ± 0.09	1.21 ± 0.10
C	0.85	1.13	0.87 ± 0.07	1.15 ± 0.09

Three vacuum glazing installed in solid wood frames were tested using a guarded hot box calorimeter. The predicted and experimentally determined overall heat transfer coefficients for the total window and centre-of-glass areas are compared in Table 3.2 [42].

Table 3.2 shows that using better coatings with reduced emittance leads to lower overall heat transfer coefficients for vacuum glazing systems. The experimentally determined overall heat transfer coefficients are in good agreement with those predicted theoretically within experimental error. Predictions indicate that a glazing with two low-e coatings of 0.04 and 0.16 will have centre of glass and total window heat transfer coefficients of 19.8% and 12.4%, respectively, less than a glazing with two low-e coatings of 0.16. Results from simulations showed that for a 400 mm by 400 mm glazing the effect of emittance on the overall heat transfer coefficient of the centre glass area is larger than that of the total window system due to the significant contribution of the frame area and edge effects.

3.2.3. Radiative heat transfer between the two glass surfaces within the vacuum space

Accurate measurements have been made to determine the radiative heat transfer between the internal surfaces of a vacuum glazing using the guarded hot plate apparatus [63]. The results calculated by Eq. (3.8), and the corresponding experimental data

for two low emittance surfaces showed that the experimental data were in close agreement with the quartic relationship given by Eq. (3.10). However, small departures existed between the experimental data and the values calculated using Eq. (3.10), due to variations of emittance affected by the wavelength dependence of the optical properties of the surfaces. The calculated departures were in good agreement with that of the experimental measurements. It can be seen that the measurement results were in excellent agreement with the results calculated from Eq. (3.8) [32,40]. In this sample, the gas conduction was known to be negligible.

3.3. Support pillar arrays

3.3.1. Pillar choice

The pillars are typically 0.25–0.5 mm in diameter and 0.1–0.2 mm in height. To date they have been positioned in a square array, separated by 20, 25, 30, and 35 mm for a glass thickness of 3, 4, 5 and 6 mm, respectively. In the designs of vacuum glazing, the pillars must be made from a material with a compressive strength of at least 1 GPa [66]. In terms of these conditions, ceramics, such as alumina, and metals, such as stainless steel and Inconel (a nickel based alloy) can be used as support pillars. Collins and Fischer-Cripps [67] have proposed 4 MPa as a tolerable level of mechanical tensile stress due to atmospheric pressure on the outside surface of glass sheets above the pillars. This value was chosen to be about one half of the maximum allowable steady tensile stress in untempered glass, as specified in glass design standards [68].

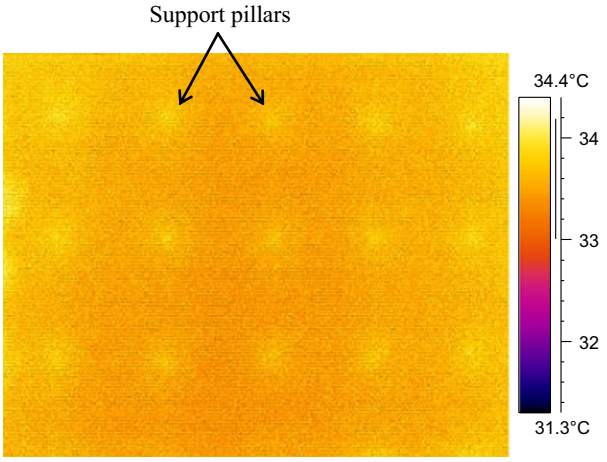

Fig. 3.4. Pillar heat transfer shown by an infrared thermography [45].

The magnitude of the stresses above the pillars is dependent on the thickness of the glass sheets. The choice of pillar dimension, separation, and thickness of the glass sheet is governed by four restrictions, which will be discussed in the stress analysis section.

3.3.2. Heat conduction through the support pillars

In most practical samples of vacuum glazing, the thermal conductivity of the pillar material ($\sim$20 W m^{-1} K^{-1} for alumina and stainless steel) is much larger than that of the glass sheets (k_{glass}=1 W m^{-1} K^{-1}) [66]. The amount of heat flow through a pillar is therefore determined by the spreading heat flow in the glass sheets and can be characterised by the pillar thermal resistance [55]:

For a single pillar:

$$C_{onepillar} = 2k_{glass}a \tag{3.12}$$

$$Q_{onepillar} = 2k_{glass}a(T_1 - T_2) \tag{3.13}$$

For a square array of conducting pillars:

$$Q_{pillararray} = \left[\frac{2k_{glass}a}{s^2}\right]\Delta T \tag{3.14}$$

The thermal conductance due to heat flow through the pillar array is given by

$$C_{pillararray} = \frac{2k_{glass}a}{s^2} \tag{3.15}$$

The pillar thermal resistance obtained by the FEM method is within 0.3% of the analytic result [66]. The calculated near-uniformity of the heat flux due to the pillar array was confirmed by an infrared thermograph measurement of the warm [66] and cold [35] side external glass surfaces. The U-value of glass-to-glass central area (U_{g-g}) contributed by pillar array $U_{pillararray}$ and long-wave radiation U_{rad} were modelled using the finite element analysis [69]. Infrared thermography of the glass surfaces as shown in Fig. 3.4 were employed to validate the predictions of the finite element analysis as shown in Fig. 3.5. The presence of a pillar reduces the temperature difference between the internal surfaces of the glass sheets in the immediate vicinity of the pillar, and thus reduces the radiative heat transfer in this region. Very good agreement was found between the estimates of heat flow obtained by the analytic approach and the finite volume method [54,45].

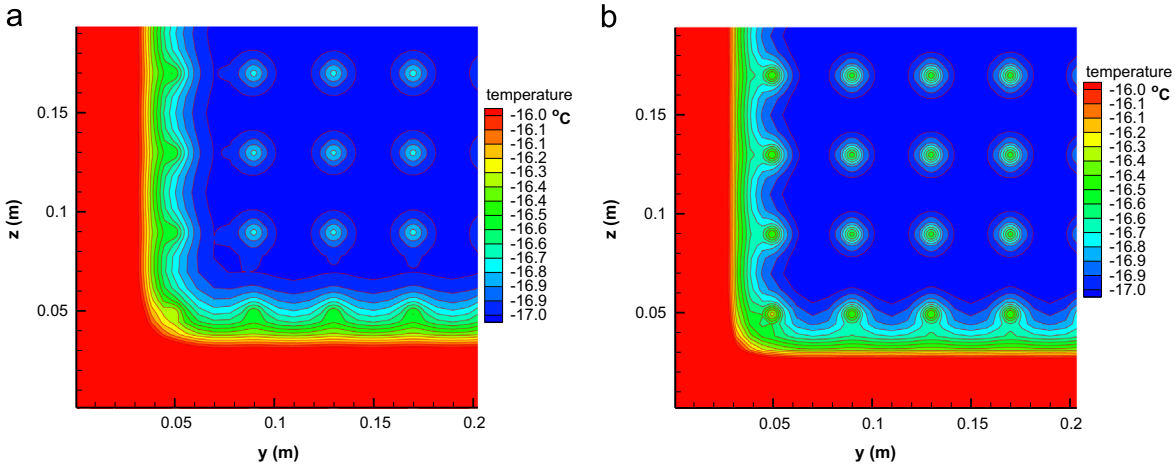

Fig. 3.5. Predicted cold side isotherms for a vacuum glazing with two 6 mm (a) and 4 mm thick glass sheets [45].

Pillar conduction gives periodic temperature variations across the external surfaces of the glazing as shown in Figs. 3.4 and 3.5. These temperature variations on the full pillar array have been studied using two methods: first, surface temperature for a single pillar obtained from the axisymmetric two-dimensional finite element model was superposed using a resistive combination method [53]. Second a three dimensional finite volume method was used to calculate the temperature profile [69,40]. The results obtained by these two approaches were essentially identical. Griffiths et al. [54,69] and Fang et al. [45] presented the detailed isotherms modelled in the regions above each support pillar. From these isotherm diagrams, it could be seen that for vacuum glazing with 4 mm and 6 mm thick glass sheets, the magnitude of the temperature variations above the pillars for each system was 0.6 °C and 0.3 °C, respectively [69,45]. This magnitude of temperature variation was sufficiently small in the case of pillars with a diameter of 0.32 mm under standard winter conditions [70], using this pillar arrangement so that water condensation above each support pillar was only likely to occur on the warm surface of the glazing under the conditions where significant condensation was already evident around the edges. This conclusion was in agreement with the observations in practical samples of vacuum glazing [24,45,66].

The results obtained from the above two approaches showed that the variations of the surface temperature due to the heat flow through the pillars were quite small, only about 4% of the total temperature difference between the external surfaces of the glass sheets [66,24]. These results were in very good agreement with the infrared thermographic measurement made on a vacuum glazing sample at the Lawrence Berkeley Laboratory, U.S.A. [55] and in the University of Ulster [54,35]. Over more than 90% of the area the heat flux density was constant within ±5%. This vindicated the approach of simulating the pillar array as a uniform slab of material with appropriate thermal conductivity in some analyses of heat transfer within vacuum glazing [32].

Setting up a small section of an evacuated glazing with an adiabatic boundary, i.e. no heat transfer through the boundary, and changing the pillar separation are illustrated in Fig. 3.6. In the small section of vacuum glazing, four pillars with diameters of 0.32 mm supported two 6 mm thick glass sheets coated with low-e coatings of emittance of 0.18 on the two interior glass surfaces. There was no edge seal and no frame insulation, the dimensions of the systems were 60 mm by 60 mm and 40 mm by 40 mm, respectively, the predicted *U*-value under ASTM conditions [70] are listed in Table 3.3 [45].

Table 3.3 shows that the change in *U*-value of the glazing area with an adiabatic boundary and different pillar spacing is significant. If using tempered glass panes in vacuum glazing, the pillar separation can be increased, e.g. for 4 mm thick tempered glass panes, the pillar separation can be increased to 54 mm [71]. The heat conduction of the pillar array can be predicted reduced by 30%.

Simulations were undertaken for different pillar diameters in a vacuum glazing with dimensions of 500 mm by 500 mm, a 3 mm wide edge seal, 14 mm high internal and external insulations, and a pillar array of 40 mm separation and 0.32 mm diameter. The two 6 mm thick glass sheets were coated with low-e coatings of 0.2 emittance on both interior glass surfaces; the results from the simulation are shown in Fig. 3.7 [45].

Fig. 3.7 shows that with increasing pillar diameter, the heat transfer through each pillar increases. The thermal conductance of the pillar array increases, so the *U*-value increases. The internal surface temperature decreases and the external average surface temperature increases. Comparing the results in Table 3.3 and Fig. 3.7, it can be seen that the influence of the pillar diameter on

Table 3.3
Thermal performance of two small sections of vacuum glazing with adiabatic boundaries and different pillar separations.

	T_2 (°C)	T_1 (°C)	C_{center} W m^{-2} K^{-1}	C_{total} W m^{-2} K^{-1}	U_{total} W m^{-2} K^{-1}
Pillar separation (mm)	30 −16.9	17.9	0.76	0.76	0.68
	20 −16.6	16.7	1.10	1.10	0.94

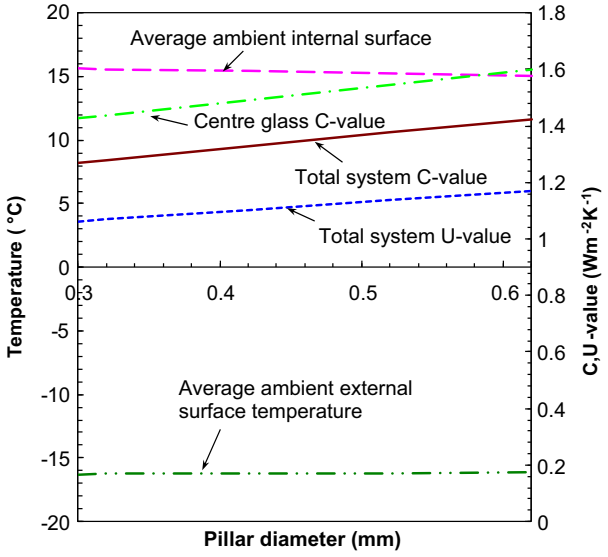

Fig. 3.7. Predicted effect of the pillar diameter on the thermal performance of an evacuated glazing with dimensions of 500 mm by 500 mm [45].

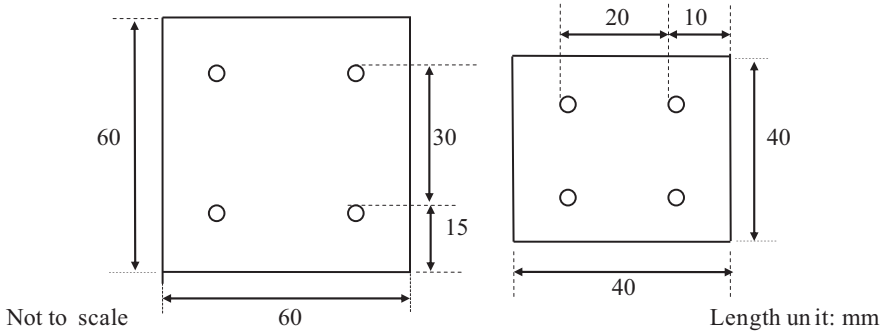

Fig. 3.6. Schematic diagrams for small sections of vacuum glazing with adiabatic boundaries and different pillar settings.

the whole vacuum glazing system is lower than that of the small glazing area with adiabatic boundaries.

3.3.3. Predicted effect of the pillar array height on the thermal performance of a vacuum glazing

Simulations of the effect of pillar height on the thermal performance of an evacuated glazing were undertaken for which the height of both internal and external frame insulation was 14 mm. The number of divisions in each horizontal plane of the evacuated glazing surface was increased from 62 to 110 resulting in 12,100 cells across each horizontal plane. There were 20 horizontal planes in the simulation of the evacuated glazing. The predicted thermal property variations due to the pillar height are shown in Fig. 3.8. The dimensions of the evacuated glazing modelled were 500 mm by 500 mm. The vacuum space between two 6 mm thick glass sheets was sealed by a 2 mm wide indium alloy edge seal, and supported by a pillar array with 40 mm separation and 0.32 mm diameter. The rebate of the frame insulation was 14 mm.

Fig. 3.8 shows that with increasing pillar height, the heat conduction path through the pillars from the internal surface to the external surface increases, therefore the total *U*-value of the glazing decreases. It can be seen however that the influence of pillar height is very small. When the pillar height increases from 0.12 mm to 0.72 mm, the heat transfer coefficient decreases by 0.008 $W\,m^{-2}\,K^{-1}$. As the pillar conductivity 20 $W\,m^{-1}\,K^{-1}$ is much larger than that of the glass sheets 1 $W\,m^{-1}\,K^{-1}$, only a very small proportion of the overall temperature difference exists between the ends of the pillar. The amount of heat flow through the pillar is therefore dominated by the spreading heat flow in the glass sheets and can be characterised by the pillar resistance [66]. It is clear that in vacuum glazing designs, the effect of pillar height on the thermal performance of evacuated glazing can be ignored [45].

3.3.4. Experimental test for heat conduction through the support pillars

The heat flow through the pillars can be obtained by deducting the radiation and residual gas conduction from the overall heat transfer. The measurement of the heat flow in a vacuum glazing sample due to radiation and gas conduction must be determined initially. This was done in experimental samples with a circular region of about 50 mm in diameter where there was no pillar. The combined heat flow for radiation and residual gas in the vicinity of the pillar was then measured. The heat flow through the pillar was determined by subtracting the combined heat flow of radiation and gas conduction from the overall heat flow measured by the guarded hot plate equipment. The influence of temperature difference reduction caused by pillar conduction was calculated by the finite element model [72,35,40]. The measured data were very close to that obtained from the analytic model Eq. (3.12). The image taken by an infrared camera was in good agreement with the predicted isotherms shown in Fig. 3.4. This provided both a strong confirmation of the accurate calibration of the measuring method and a validation of the modelling procedure.

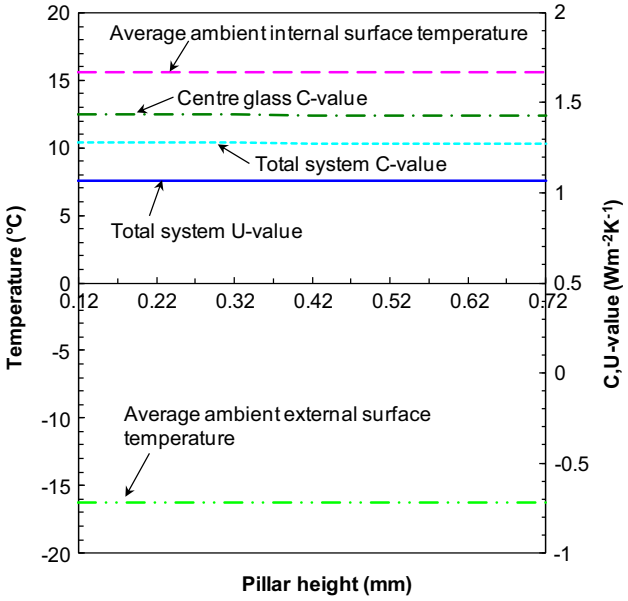

Fig. 3.8. Predicted effect of the pillar height on the thermal performance of a vacuum glazing. The rebate depth of the frame insulation was 14 mm [45].

3.4. Frame and the residual gas within a vacuum glazing

3.4.1. Frame functions

In all vacuum glazings, heat flows along the glass sheet and through the thermally short-circuiting contiguous edge seal from the warm side to the cold side glass sheet. The USD has modelled the heat transfer through the edge seal by two ways [53]. First, a simple analytic model was used in which temperature variation through the thickness of each glass sheet was ignored. Second, a three-dimensional finite element model (FEM) was employed. In both methods, the pillar array was modelled as a uniform slab of material with appropriate thermal conductivity, and external heat transfer was approximated by uniform conductance. The two methods gave results which were in excellent agreement. The analytic model provided a very simple method to calculate the magnitude of the heat transfer due to the edge effect. At the UU, the heat transfer through the edge was simulated using a finite-volume model based on the "unified model" [73]. The results validated experimentally were similar to those of the USD [54,74,35,40]. Complex multi-material frame was designed and constructed at the UU. The experimentally achieved and predicted *U*-values and temperature profiles were in good agreement, which is detailed in [34].

The insulating frame has two important effects on the vacuum glazing thermal performance. First, it reduces the *U*-value of vacuum glazing, since the increased frame recess depth increases the lateral heat conduction along the glass sheet and through the edge seal. Second, it raises the temperature of the glass at the edge relative to the mean temperature of the entire glazing. This reduces the thermal tensile stress in the edge region of each glass sheet. Consequently, the probability of glazing failure reduces [53,34].

3.4.2. Complex multimaterial frame design

A frame must provide high thermal insulation and maintain the structural strength and rigidity to support an evacuated glazing over its serviceable life. Since the thermal conductivity of many thermal insulations are much lower than those of common frame materials, the inclusion of an insulation within the frame was considered. To provide frame rigidity and combat the inherent low mechanical strength and rigidity of insulation, they were placed in an exoskeleton structure made of common frame materials. The geometrical configuration of the exoskeleton frame shown in Fig. 3.9 was selected on the basis of strength and ease of manufacture. Aluminium, wood, polypropylene, polyethylene, polyvinylchloride or Teflon® may be used to form the exoskeleton structure, with a range of solid thermal insulations filling the internal cavities. The heat transfer coefficient of a vacuum glazing with a solid polypropylene or wood frame and a complex

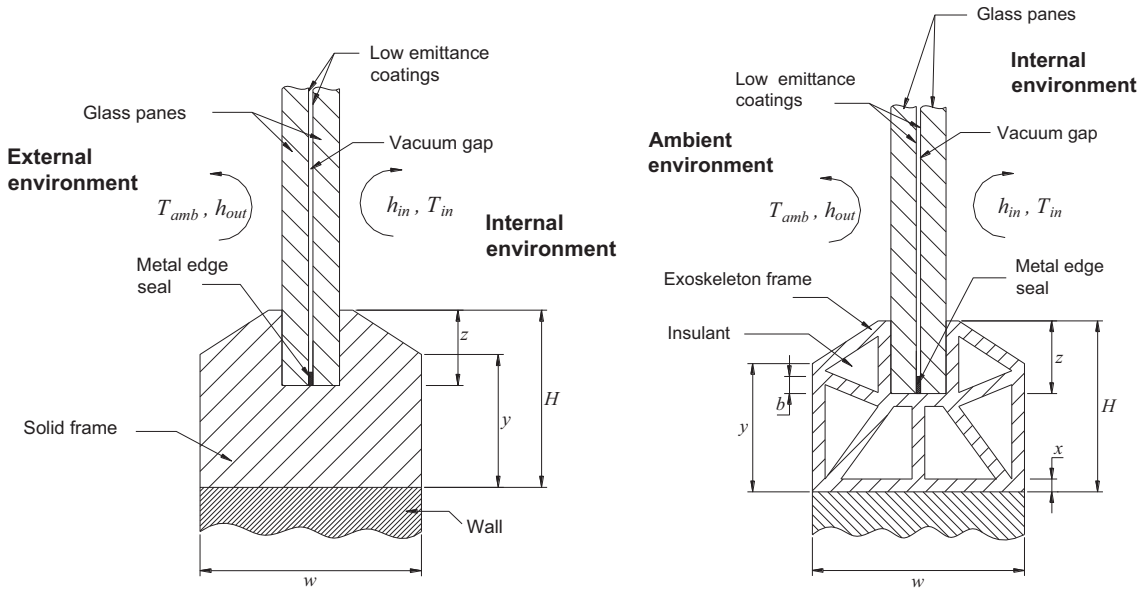

Fig. 3.9. A complex multimaterial window frame housing an evacuated glazing with a metal-based edge seal.

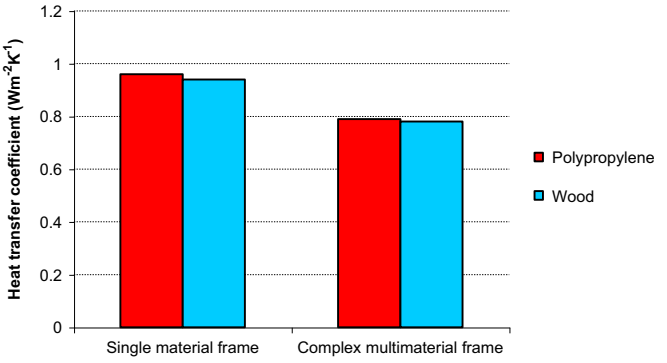

Fig. 3.10. Thermal performance of a vacuum glazing with a solid polypropylene or wood frame and a complex multimaterial frame with either a polypropylene or wood exoskeleton framework.

multimaterial frame with either a polypropylene or wood exoskeleton framework are shown in Fig. 3.10 which shows that the inclusion of a multimaterial frame lead to a reduction of heat transfer coefficient by 20%.

The isotherms of the non-thermally-broken and thermally-broken aluminium complex frame are illustrated in Fig. 3.11. The widths of the two rubber thermal breaks in this simulation were 2.3 mm and 4.7 mm. The insulation material within the cavities of the frame was expanding foam. The predicted thermal performance with different thicknesses of both non-thermally-broken and thermally-broken aluminium exoskeleton frames with an expanding foam insulation infill are illustrated in Fig. 3.12 [34].

Comparing Fig. 3.11(a) and (b), the influence of the thermal break on the temperatures across the glazing can be seen. The complex multimaterial frame with the thermal break increases the temperatures of the glass area on the hot side by 1.8 °C, and decreases the temperature of the glass area on the cold side by 0.5 °C.

The influence of aluminium exoskeleton on the thermal performance of the vacuum glazing is presented in Fig. 3.12, which shows that increasing the exoskeleton framework thickness results in increasing the heat transfer coefficient through the frame area while that through the glass areas remains almost constant. For an aluminium frame either with or without thermal break, the rate of increase in the heat transfer coefficient of the overall window system decreases with increasing framework thickness, i.e. the effect of the exoskeleton thickness on the thermal performance of the overall evacuated glazing window system decreases. Modelling of vacuum glazing system showed that when the aluminium exoskeleton thickness increases from 0.5 mm to 3 mm, the increase in the heat transfer coefficient of the overall window is 0.23 W m^{-2} K^{-1} and 0.08 W m^{-2} K^{-1} for the frame with and without thermal break, respectively. The corresponding increase in the heat transfer coefficient of the frame area was 305.15 W m^{-2} K^{-1} and 4.72 W m^{-2} K^{-1} and the increase in the heat transfer coefficient of the exposed glass area was 0.06 W m^{-2} K^{-1} and 0.04 W m^{-2} K^{-1} for the frame with and without thermal break, respectively. Although the increase in the heat transfer coefficient of the frame area is large especially for the non-thermally broken aluminium frame, when the width increases from 0.5 mm to 3 mm, the increase in heat transfer coefficient of the overall window system is only 0.23 W m^{-2} K^{-1}. The heat transfer disadvantage associated with a thicker aluminium exoskeleton frame are not sufficient to prevent its use if required to maintain strength and rigidity in the window system. When using non-thermally-broken aluminium frames, the risk of condensation on the aluminium frame surface is significant [75].

3.4.3. Heat conductance through the residual gas within the vacuum space

When the vacuum within the glazing degrades to a value of larger than 1 Pa, the heat transport through the vacuum space cannot be neglected [50]. Heat transfer in residual gas between the glass sheets occurs in one of three ways.

- First, in this circumstance, the mean free path for molecule–molecule collisions is small compared with the distance over which heat is transported, the rate of the heat flow through the gas is independent of pressure. For two parallel plane surfaces of area A and separation of d, the rate of heat transport in this so-called viscous flow region is

$$Q_{\text{viscous}} = \frac{k_{\text{gas}} A(T_1 - T_2)}{d} \tag{3.16}$$

[50], where T_1 and T_2 are the temperatures of the two surfaces.

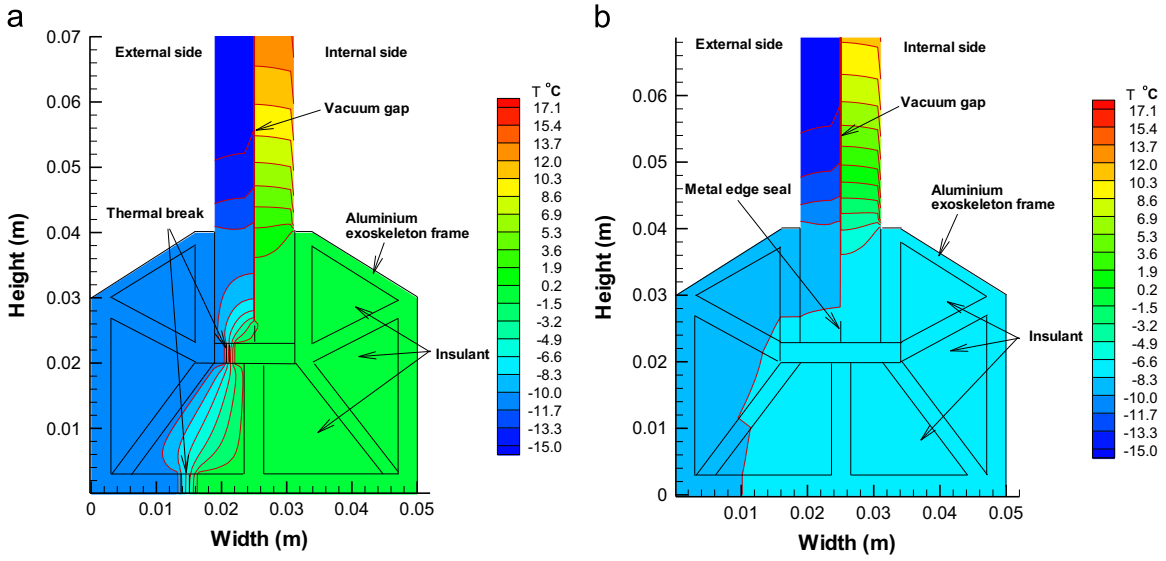

Fig. 3.11. Isotherms comparison between the aluminium exoskeleton frames with (a) and without thermal break (b).

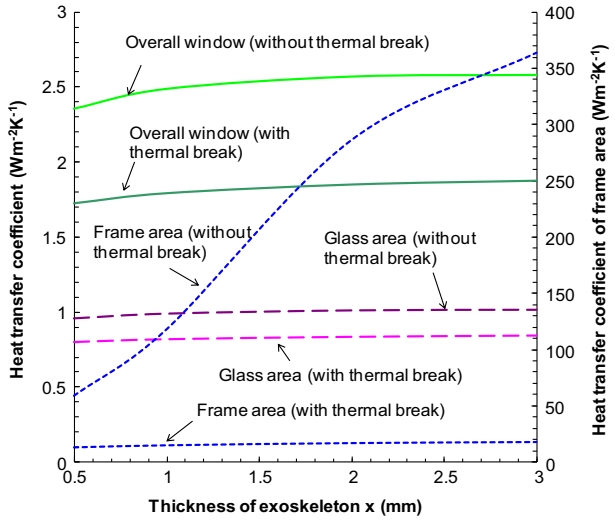

Fig. 3.12. Thermal performance of a vacuum glazing with aluminium exoskeleton thicknesses in the range 0.5–3 mm for a non-thermally-broken and a thermally-broken complex multimaterial frame.

- Second, in the molecular flow region, the mean free path is large compared with the distance of the heat flow. For vacuum glazing with 0.2 mm vacuum space, this pressure is 30 Pa or 3×10^{-4} atm. The rate of the heat flow is proportional to pressure P [50].

$$Q_{\text{molecular}}=\alpha\left[\frac{(\gamma+1)}{(\gamma-1)}\right]\left[\frac{B_m}{8\pi MT}\right]^{1/2}PA(T_1-T_2). \tag{3.17}$$

In this expression, B is the combined accommodation coefficient given by

$$\alpha=\frac{\alpha_1\alpha_2}{[\alpha_1+\alpha_2-\alpha_1\alpha_2]}, \tag{3.18}$$

The magnitude of the heat flow depends on the gas species, and on the effectiveness of the energy exchange between individual molecules and the surface as given by the accommodation coefficients. In vacuum glazing, water vapour was determined to be the major gas species in the internal space of the glazing [76]. Water molecules interact strongly with the internal surfaces of the vacuum glazing. Assuming a combined accommodation coefficient of 0.9, the gaseous conductance at the low pressure is approximately equal to $0.8P$. In order to ignore gas conduction, the pressure within the glazing should be less than 0.1 Pa [32].

- Third, in this case, the mean free path is comparable with the heat transport distance. It was found experimentally [77] that the rate of the heat flow in this region can be approximated as

$$\frac{1}{Q_{\text{gas}}}=\frac{1}{Q_{\text{viscous}}}+\frac{1}{Q_{\text{molecular}}}, \tag{3.19}$$

where $Q_{\text{molecular}}$ is given by Eq. (3.17) at the pressure of interest. In a vacuum glazing, Eq. (3.17) can be used to analyse the heat conduction. In some ageing experiments, however, the gas pressure might be increased to the intermediate region, and Eq. (3.17) provides a method to estimate the gas pressure from heat transfer measurements.

Table 3.4
Overall heat transfer coefficients of central glass and total window areas of two vacuum glazing samples.

Vacuum glazing no.	Predicted U-values ($\text{W m}^{-2}\text{K}^{-1}$)		Experimentally determined U-values ($\text{W m}^{-2}\text{K}^{-1}$)	
	U_{centre}	U_W	U_{centre}	U_W
1	1.00	1.19	0.97 ± 0.08	1.21 ± 0.10
2	0.90	1.10	1.06 ± 0.09	1.28 ± 0.11

A 2-D finite element model was used to predict the temperature profiles along the central lines of vacuum glazing [35,40]. The thermal conductivity of the vacuum gap was determined by the combined contribution of support pillars (Eqs. 3.12–3.15), radiative heat flow (Eqs. 3.5–3.11) and residual gas (Eqs. 3.16–3.19). Thermal performance of two vacuum glazing were tested using a guarded hot box calorimeter and the temperature profiles were modelled and presented in Table 3.4 and Figs. 3.13 and 3.14.

For sample 1, the overall heat transfer coefficient of the central glass region of the sample was experimentally determined to be $0.97\pm0.08\ \text{W m}^{-2}\text{K}^{-1}$. The measured and predicted U-values and

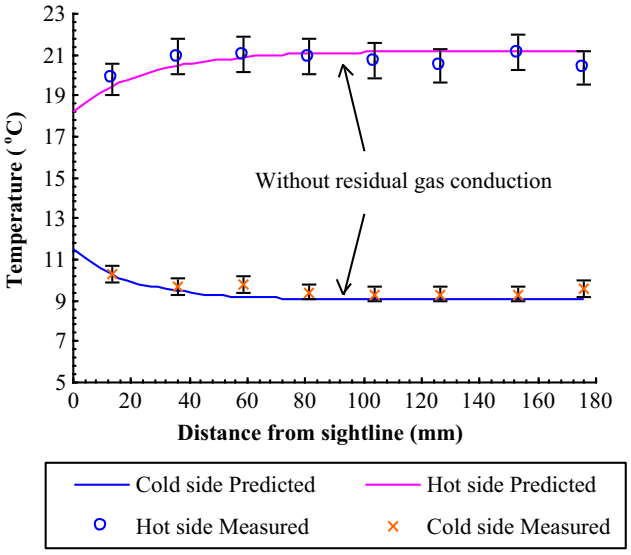

Fig. 3.13. Measured and predicted glass surface temperature profiles along the centre lines of vacuum glazing sample 1 rebated 20 mm into a solid wood frame.

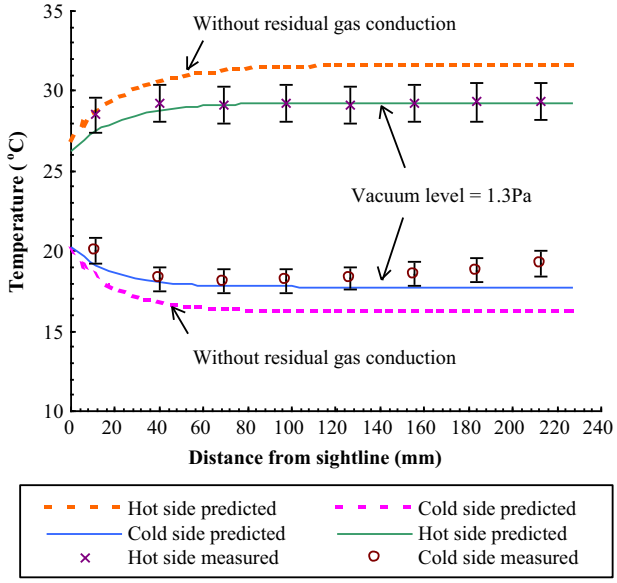

Fig. 3.14. Measured and predicted glass surface temperature profiles along the centre lines of vacuum glazing 2 rebated 20 mm into a solid wood frame (Fang et al., 2006).

mean surface temperatures of the vacuum glazing are in good agreement within experimental error of 5%. For sample 2, the *U*-value of the centre-of-glass region was experimentally determined to be 1.06 ± 0.09 W m^{-2} K^{-1}. The residual gas pressure within the evacuated space was determined to be less than 0.1 Pa for sample 1 and 1.30 Pa for sample 2 [35].

3.4.4. *Heat conduction through the residual gas in the vacuum space*

It is important to determine the level of vacuum in an as-produced sample of vacuum glazing, and to identify the degradation mechanisms during ageing. However it is difficult to separate the contributions made to the heat flow by radiation and gas conduction in a sealed sample.

In an as-produced vacuum glazing sample, measuring the rate of the heat flow through the sample as a function of the temperature difference across the sample is a convenient and non-destructive method. It can be seen from Eqs. (3.5) and (3.17) that the dependencies of heat flow on radiation and gas conduction are different. In order to investigate these two different functions, the guarded hot plate apparatus was used to measure the heat flow as a function of temperature difference across the sample of vacuum glazing. If the results from the measurement closely reflect the temperature dependence of $T_1^4 - T_2^4$, which is identical to the results from Eq. (3.5) where the emittances are independent of wavelength, the residual gas conduction can be neglected.

A sample of vacuum glazing made of hard low-e coated glass panes (*K*-glass) was heated for about 100 days at 100 °C. The thermal conductance of this aged sample increased by 0.33 W m^{-2} K^{-1} compared to that measured at room temperature before the ageing experiment [32]. The measurements' departure from the $T_1^4 - T_2^4$ dependence are much larger than the errors in the measurements. This proved that after high temperature ageing, the vacuum within the sample was degraded. The relative heat flow due to each process obtained in this way agreed closely with the radiative and gaseous conductance obtained from measurements on the sample before and after ageing, respectively. This technique is therefore a useful, non-destructive diagnostic test of vacuum glazing durability since it provides a reasonably sensitive indication of the presence of gas without destroying the sample.

At the UU, a vacuum glazing of 0.4 m by 0.4 m with a *U*-value of 1.0 W m^{-2} K^{-1} was subjected to extreme thermal cycling resulting in significant thermal gradients over the glazing [39]. In a guarded hot box calorimeter an air temperature of 22 °C was maintained in the metering box while in the environmental box air temperature was cycled over 8 h between −30 °C and 50 °C for 15 cycles. After thermal cycling it was found that the thermal conductance of the whole vacuum glazing had increased from 1.22 W m^{-2} K^{-1} to 1.32 W m^{-2} K^{-1} while the centre of the pane, glass to glass heat conductance increased from 1.18 W m^{-2} K^{-1} to 1.30 W m^{-2} K^{-1}. Using the model for heat conduction in a vacuum, it was determined that the vacuum pressure within the evacuated gap increased from 0.1 Pa to 0.16 Pa which is approaching the upper limit of the range developed by Collins and Simko [32], for which the residual gas contribution to the thermal performance of a vacuum glazing can be neglected. The degradation of vacuum pressure determined by this model agreed well with the glass surface temperature difference predicted using a finite element model. In a significant difference to vacuum glazing manufactured with a solder glass edge seal, no significant glass pane bending was observed and shear fracture adjacent to the pillars did not occur after the indium alloy based vacuum glazing was subject to a large temperature differential. Vacuum glazing fabricated with an indium alloy edge seal can accommodate large temperature differentials.

The major conclusions from the work of Collins and Simko [32] and Fang et al. [39] are as follows:

- level of gas conductance in most freshly manufactured samples of vacuum glazing was extremely small,
- increase of the thermal conductance of a sample which had been degraded by ageing at elevated temperature was due to an increase in gas pressure within the sample, and
- emittance of pyrolitically deposited low emittance coatings appeared to be unaffected by the ageing procedures which were employed.

3.5. *Thermal performance of overall vacuum glazing*

3.5.1. *The predicted thermal performance of vacuum glazing with different dimensions*

The dimension of an evacuated glazing is a main factor that influences the thermal performance of the glazing system. This is

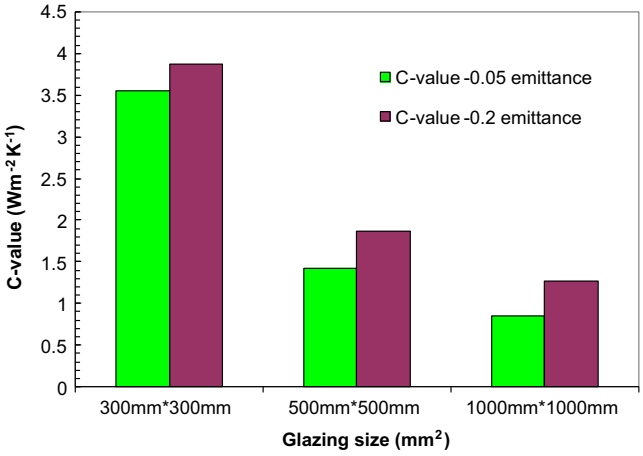

Fig. 3.15. Heat conductance comparison of vacuum glazing with different dimensions. The three glazings consisted of 4 mm thick glass sheets, 10 mm wide edge seal, 25 mm pillar spacing and 0.32 mm pillar diameter. No frame insulation was employed.

because the heat transfer through the area close to the edge seal and centre-of-glass region are quite different. The heat transfer coefficient in the centre-of-glass area is less than that in the region close to the edge area. Thermal performance of three evacuated glazings with three different sizes was simulated using the finite volume model. The three evacuated glazing consisted of two 4 mm thick glass sheets supported by a pillar array with a 0.32 mm diameter and spaced at 25 mm, and sealed by a 10 mm wide edge seal. The emittances of low-e coating on the two interior surfaces were 0.05 and 0.2, respectively. No frame insulation was employed. The predicted thermal performances of the three glazing systems are presented in Fig. 3.15 [38].

Fig. 3.15 shows that with increasing dimensions of a vacuum glazing, the heat transfer coefficient of the glazing system decreases, i.e. the larger the vacuum glazing, the better the thermal performance of the glazing system will be. When the dimensions of evacuated glazing increase from 300 mm by 300 mm to 1000 mm by 1000 mm, the heat transfer coefficient reduces by about 2.6 W m^{-2} K^{-1} under the simulation conditions. The indium alloy edge seal is a short circuit for heat transfer. The heat transfer through the edge seal is much larger than that through the centre-of-glass area. When the dimensions of an evacuated glazing increase, the ratio of heat transfer through the edge seal to the heat transfer through the overall glazing system decreases.

In Fig. 3.15 when the emittances of low-e coatings on the interior surfaces of vacuum glazing increased from 0.05 to 0.2, for the 0.3 m by 0.3 m vacuum glazing system, the heat transfer coefficient of the vacuum glazing increased by 0.32 W m^{-2} K^{-1}. For the 0.5 m by 0.5 m and 1 m by 1 m vacuum glazing systems, the heat transfer coefficient of the vacuum glazing increased by 0.40 W m^{-2} K^{-1}. Therefore the low-e coatings improved the thermal performance of a vacuum glazing with a larger size more efficiently than that of glazing with a small size.

3.5.2. Total heat transfer through a vacuum glazing system

The total thermal conductance between the glass sheets of a vacuum glazing can be determined by combining the heat flows due to gas conduction, radiation, and pillar conduction with the influence of external heat transfer process [32]:

$$C_{\text{glass-glass,centre-of-glazing}} = C_{\text{glass-glass,gas}} + C_{\text{glass-glass,radiation}} + C_{\text{glass-glass,pillars}} \quad (3.20)$$

$$= 0.8P + 4\varepsilon_{\text{effective}}\sigma T^3 + \frac{2k_{\text{glass}}a}{s^2} \quad (3.21)$$

In a well-made vacuum glazing (gas pressure < 0.1 Pa), the gas conduction can be ignored [32].

The total air-to-air thermal conductance of a vacuum glazing can be obtained by combining the conductance in the central glass area and the edge glass area. In the central glass area, the conductance is calculated simply by combining the internal conductance in series with the external heat transfer coefficients:

$$\frac{1}{U_{\text{air-air,centre-of-glazing}}} = \frac{1}{h_{\text{air-glass}}} + \frac{1}{C_{\text{glass-glass,centre-of-glazing}}} + \frac{1}{h_{\text{glass-air}}} \quad (3.22)$$

Near the edge area, the air-to-air heat flow associates with lateral heat flow near the edges. For a rectangular glazing with dimensions of c by d, if the effect of the corners is ignored, the edge conductance can be estimated from Eq. (3.23) as:

$$U_{\text{air-air,edge}} = \frac{(2(c+d)/cd)k_{\text{glass}}t}{\left(\sqrt{k_{\text{glass}}t/h_1} + w_1 + w_2 + \sqrt{k_{\text{glass}}t/h_2}\right)} \quad (3.23)$$

Adding the contributions from the centre-of-glazing (Eq. (3.22)) and the edges (Eq. (3.23)), the total air-to-air thermal conductance of the vacuum glazing is obtained by Collins and Simko [32]:

$$U_{\text{air-air,total}} = U_{\text{air-air,centre-of-glazing}} + U_{\text{air-air,edge}} \quad (3.24)$$

3.5.3. Total heat transfer through a vacuum glazing

The method for determining overall heat transport outlined in Section 3.5.2 has been validated by experimental data. The overall heat transport through a vacuum glazing has been measured using the guarded hot box method [35,78,79]. The vacuum glazing was mounted in a mask wall, which divided the hot box into two chambers: a cold chamber and a warm chamber. The temperature was well-controlled in the warm chamber at 20 ± 0.1 °C. In the cold chamber, the temperature could be set to any value between 0 ± 0.1 °C. Heat transfer coefficient from both sides and the edge losses through the mounting structure were controlled to precise values. The experimental measured U-values were in excellent agreement with the calculations made in Section 3.5.2. The estimates of the heat transport based on the measurements of the local heat flow were within a deviation of $\pm 6\%$ [35,40,79].

The overall heat transport was also determined by local heat flow measurement and calculations using the analytic model [79]. The experimental samples of vacuum glazing were made with a pillar-free region about 50 mm in diameter. The modelling results showed that the contribution from pillars to the heat flow near the centre of this region was negligible. Local heat flow through a few individual pillars was measured, then the total individual heat flow were determined using the modelling data. Total heat flow through the pillar array was obtained by multiplying the average individual pillar conductance by the number of pillars.

The total centre-of-glazing U-value was obtained by combining the radiative and pillar array heat transfer coefficients. Using this value, the total heat flow $Q_{\text{radiation+pillars}}$ through the centre-of-glazing area was determined. Because of the heat conduction through the edge seal, the temperature difference in the area close to the edge seal was less than that in the area remote to the edge. In the area close to the edge, the reduction of the heat conductance by radiation and pillar conduction due to the edge effect was about 10% of the total heat flow through the vacuum

glass area [35,79], therefore the heat transfer through this area close to the edge was $0.9Q_{\text{radiation+pillars}}$. The distance of this area from the edge was called characteristic distance given by $(k_{\text{glass}}t/h)^{1/2}$. Heat flow by edge seal conduction Q_{edge} was calculated using the analytic model outlined in Section 3.1.2. The lateral heat flow along the glass sheets and through the edge seal Q_{lateral} was determined from the simple solution of the one-dimensional analytic mode. The sum of these heat flows $0.9Q_{\text{radiation+pillars}}$, Q_{edge} and $Q_{\text{lateralflow}}$ was the overall heat flow through the whole glazing system [79,40].

To summarise, techniques have been developed to estimate the magnitude of the contributions to the heat flow from several different sources: gas conduction (usually negligible), radiation, pillar conduction, and lateral heat flow in the vicinity of the edge seal. A method has been developed to combine these heat flows to estimate the overall air-to-air heat flow through a vacuum glazing. Results obtained by this method were in excellent agreement with the measurements of total heat transport through overall area of vacuum glazing samples made with an accurately calibrated guarded hot box. An important conclusion was that, to a very good approximation, the contribution to the overall heat flow from the pillars could be accurately determined by replacing the array of discrete pillars with a uniform slab of material which has an appropriate thermal conductance [32].

The infrared picture as shown in Fig. 3.2 taken by an infrared camera show the heat flow thought the support pillars, edge areas and frame. This experimentally validated the calculation method of characteristic distance: $(k_{\text{glass}}t/h)^{1/2}$ developed by the finite element model.

3.5.4. *Thermal performance of vacuum glazing as a function of insolation incident on the external glazing surface*

Insolation incident on the external surface of an evacuated glazing affects its thermal performance. The predicted thermal performance of a vacuum glazing as a function of insolation intensity is shown in Fig. 3.16. The simulated 500 mm by 500 mm vacuum glazing consisted of two 6 mm thick glass sheets with low-e coatings of 0.2 emittance sealed by a 2 mm wide indium alloy edge seal, and supported by a pillar array with pillar separation of 40 mm and diameter of 0.32 mm. The frame insulation height for both the internal and external surfaces was 50 mm, which is the typical frame height used in practical engineering designs.

It can be seen from Fig. 3.16 that with increasing insolation intensity, both the internal and external average glass surface temperatures increase due to absorbed solar energy. The internal average glass surface temperature increases at a greater rate than that of the external average glass surface temperature as the heat transfer from the inner glass sheet to the outer glass sheet decreases. When the insolation increases to over 300 W m^{-2}, the predicted average internal surface temperature increases to 21.6 °C, which is higher than the indoor air temperature of 21.1 °C, as shown in Fig. 3.16. The vacuum glazing is now a heat source, transferring heat to the internal room air.

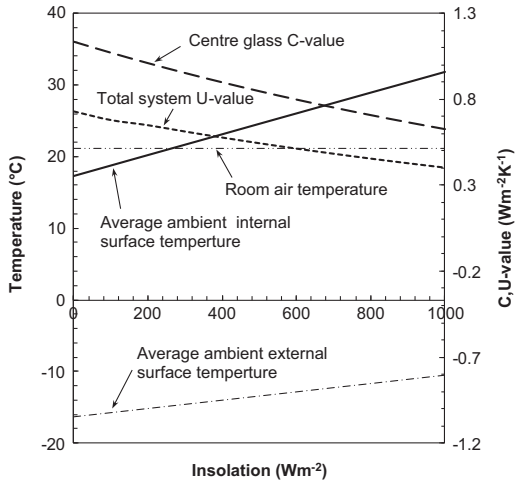

Fig. 3.16. Predicted effect of insolation on the thermal performance of an evacuated glazing. Both the internal and external insulation height was 50 mm, which is the typical frame height used in the current glazing design.

4. Comparison of two and three-dimensional finite volume models

The finite volume model (FDM) employed leads to a sparse well structured system of equations that can be efficiently solved [80]. This enables a large number of volumes to be employed to represent the vacuum glazing geometry and allows the direct representation of the small pillars. The equation bandwidth using the finite volume method is smaller than that obtained for the finite element method using 24 node brick elements and consequently requires fewer numeric operations and less CPU time to obtain a satisfactory solution. Due to symmetry conditions, only one quarter of the vacuum glazing was simulated to represent the whole glazing system under the conditions of an ASTM [70] experimental test. In the 3-D finite volume model, the support pillars were integrated and modelled into the complete system in order to make the computation easier. The cylindrical pillars employed in the real vacuum glazing structure were replaced by the same number of cubical pillars with the same cross sectional area since both pillar shapes conduct similar amounts of heat under the same boundary conditions [81]. The length of the square base of each cubical pillar is $\sqrt{\pi}a$, where a is the radius of the equivalent cylindrical pillar. A graded mesh is used with a high density of nodes in and around each pillar to provide adequate representation of the heat transfer.

In order to test the accuracy of simulations with specified mesh number, the thermal performance of a small central area (25 mm by 25 mm) with a single pillar in the centre was simulated using a mesh of $50 \times 50 \times 25$ nodes. The mesh was denser in the area close to the pillar. The 25 nodes were distributed in a graded mesh through the glazing thickness of 8.12 mm. The thermal conductance of this simulated unit with a pillar in the centre was in good agreement with the analytic prediction with 0.8% variation which is comparable to the result of Wilson et al. [66]. This level of agreement indicates that the density of nodes is sufficient to simulate the realistic level of heat flow with high accuracy [40]. The 3-D isotherms of vacuum glazing modelled at ASTM winter conditions by a finite volume model are presented in Fig. 4.1. The isotherms of the indoor and outdoor glazing surface extracted from the 3-D isotherms are shown in Fig. 4.2. The temperature profiles along the lines AA, BB and CC extracted from Fig. 4.2 are shown in Fig. 4.3. The temperature profiles calculated by the 2-D finite element model are compared in Fig. 4.4.

Fig. 4.4 shows that the temperature profiles of the vacuum glazing measured by the guarded hot box calorimeter and simulation results along the central lines of the vacuum glazing are in very good agreement. This validated the predicted temperature profiles calculated by the 2-D and 3-D finite element models.

5. Determination of pillar dimensions

In practical evacuated glazing design, stress within the glazing must be considered. The pillar separation, pillar radius and

glass thickness should be determined from the following four restrictions [32]:

- conical indentation fractures do not occur;
- compressive stress in pillars is less than a certain value, which is determined by the pillar material. For pillars of stainless steel material, this value is 1.3 GPa.
- maximum external tensile stress above pillars is less than 4 MPa.
- thermal conductance of the pillar array is less than a given value. The minimal value of the thermal conductance is determined by Eq. (5.1) [32] with the greatest pillar separation and the smallest pillar radius that satisfies the above three stress related design criteria.

$$C_{\text{pillar,array}} = \frac{2k_{\text{glass}}a}{s^2} \tag{5.1}$$

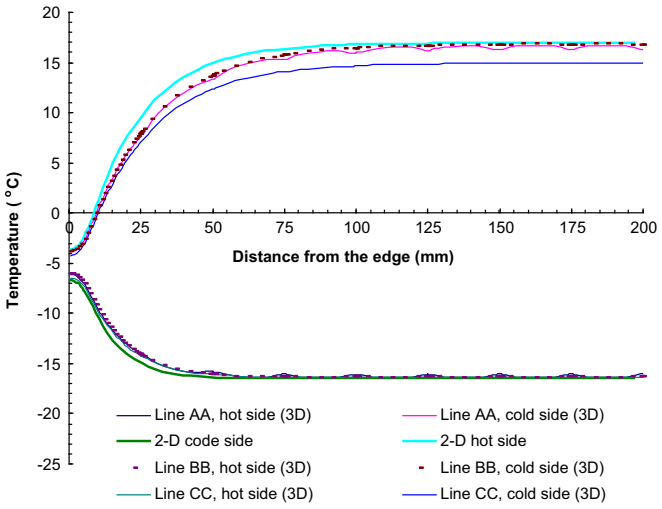

Fig. 4.3. Temperature profiles predicted by the 2-D and 3-D models along the lines AA, BB and CC as shown in Fig. 4.2 [40].

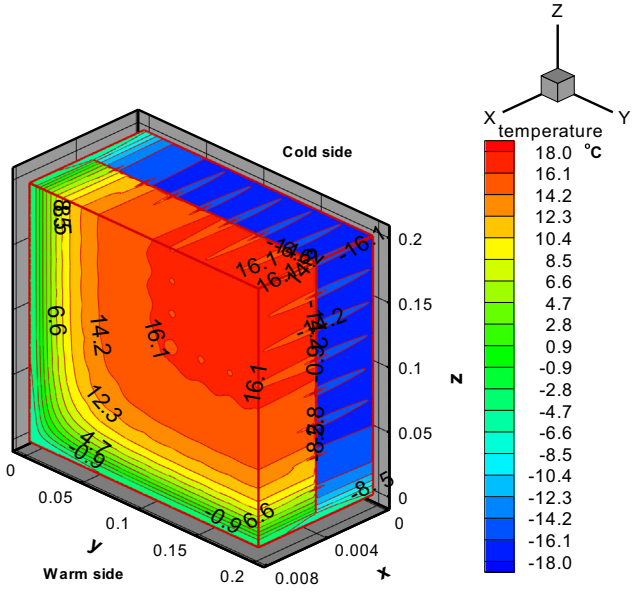

Fig. 4.1. Predicted 3-D isotherms are vacuum glazing under ASTM boundary conditions. No frame was used [40].

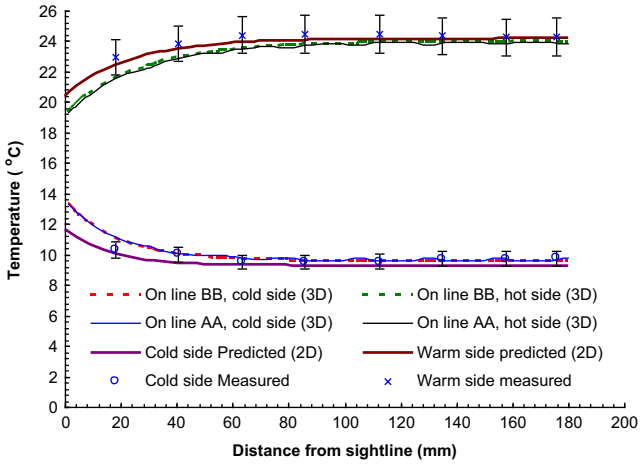

Fig. 4.4. Comparison of the experimentally determined temperature profiles along the line AA on the glazing surface to those predicted by the 2-D and 3-D models [40].

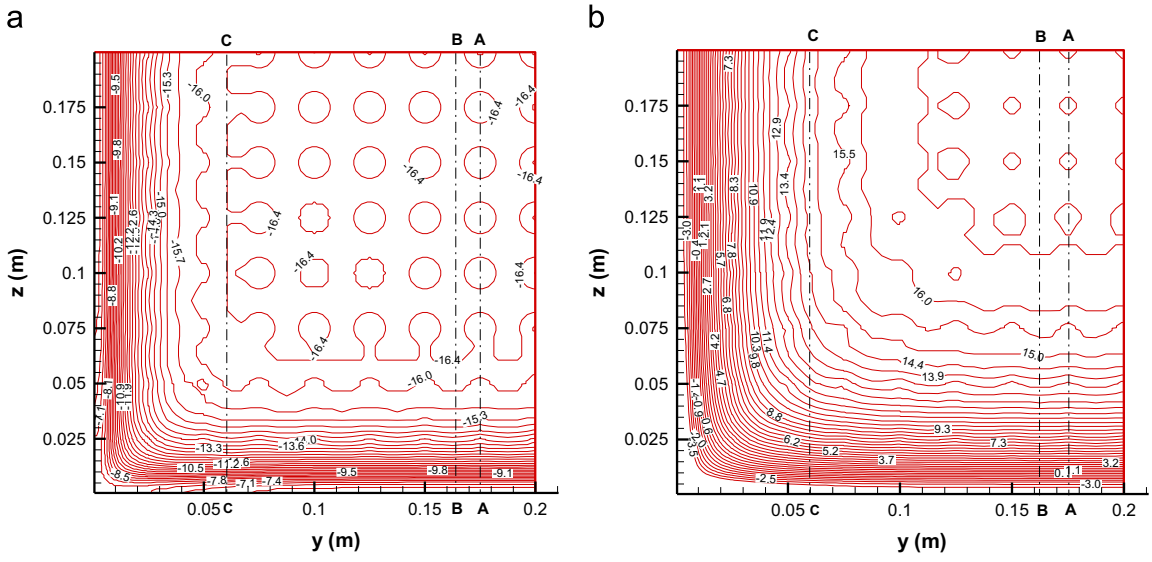

Fig. 4.2. Predicted isotherms of vacuum glazing on the cold (a) and hot (b) surfaces extracted from the 3-D isotherms. No frame insulation was used [40].

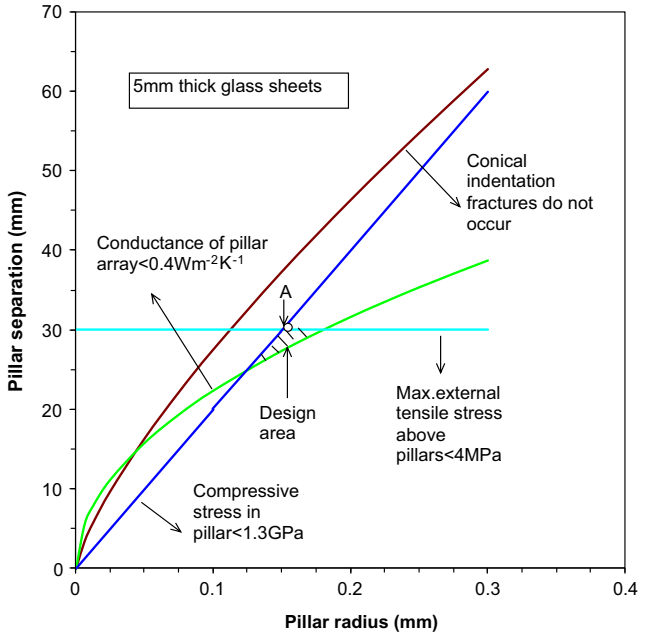

Fig. 5.1. The design process for the pillar array in an evacuated glazing. The evacuated glazing consisted of two 5 mm thick glass sheets coated with low-e coatings of emittance of 0.2, and supported by a pillar array. For the design point "*A*" the corresponding conductance of the pillar array was 0.34 W m^{-2} K^{-1}, the pillar radius was 0.15 mm and the pillar separation was 30 mm.

Table 5.1
Pillar radius, pillar separation and minimal conductance of pillar array commensurate to different glass pane thicknesses [45].

Glass pane thickness (mm)	Pillar radius (mm)	Pillar separation (mm)	Minimal conductance of pillar array (W m^{-2} K^{-1})
2	0.08	15	0.70
3	0.10	20	0.50
4	0.13	25	0.40
5	0.15	30	0.34
6	0.16	35	0.30

The design process for pillar separation, pillar radius and minimal conductance of pillar array are illustrated in Fig. 5.1.

Thermal performance of evacuated glazings with different dimensions of 0.3 m by 0.3 m, 0.5 m by 0.5 m and 1 m by 1 m was simulated. Using the four design criteria [32] for 3 mm, 4 mm, 5 mm and 6 mm thick glass sheets, the values of pillar separation, pillar radius and minimal conductance of pillar array were determined and are listed in Table 5.1 which corresponds to the point A in Fig. 5.1 for 5 mm thick glass pane as an example.

6. Thermal performance of an evacuated glazing with different glass pane thicknesses

6.1. Finite volume model analysis

In simulations undertaken, the glass sheet thickness varied but the pillar separation was constant. The predicted thermal performance variations with changing the thickness of glass panes are shown in Fig. 6.1.

Fig. 6.1 shows that the *U*-value of the 0.5 m by 0.5 m evacuated glazing increases with increasing the thickness of glass panes when using a constant pillar separation. The average internal glass

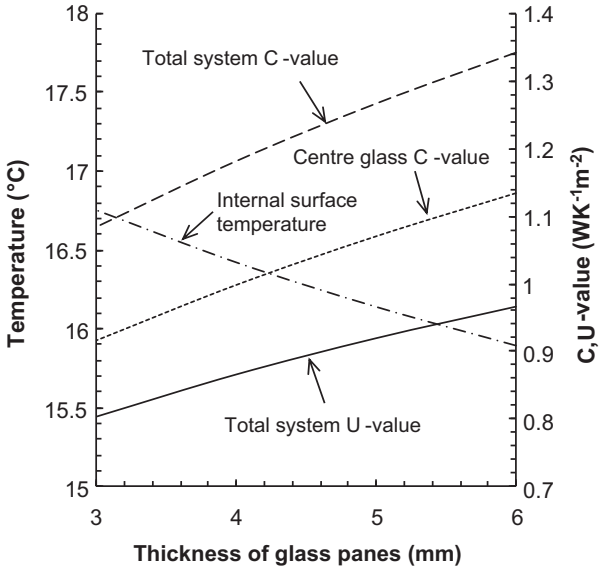

Fig. 6.1. Thermal performance variation due to changing thickness of glass panes [41].

surface temperature decreases and the heat transfer rate through the full glazing system increases.

6.2. Analytical approach

The heat flow per unit length of edge due to edge conduction is given by Simko [53]:

$$Q_{\text{edge}} = \frac{kt(T_i - T_0)}{w_1 + w_2 + \sqrt{kt/h_i} + \sqrt{kt/h_0}} \tag{6.1}$$

The heat transfer resistance and *U*-value through one pillar is given by Wilson [66]:

$$R_{\text{air-to-air}} = \frac{1}{h_i A} + \left[\left(\frac{2t}{k_g A} + \frac{1}{h_{\text{rad}} A} \right)^{-1} + 2k_g a \right]^{-1} + \frac{1}{h_0 A} \tag{6.2}$$

$$U_{\text{one,pillar}} = \frac{1}{(R_{\text{air-to-air}} A)} \tag{6.3}$$

The rate of the heat transfer per unit length of the edge calculated using Eq. (6.1) corresponding to different glass pane thicknesses *t* is presented in Fig. 6.2. The heat transfer rate through a single pillar calculated using Eqs. (6.2) and (6.3) is also shown in Fig. 6.2. The heat transfer rate through the glazing system and the *U*-value of the glazing system calculated using the finite volume model is included.

It can be seen from Fig. 6.2 that for the 0.5 m by 0.5 m evacuated glazing with increasing glass sheet thickness, the air-to-air *U*-value through a single pillar decreases, since increasing glass thickness increases the thermal resistance of the two glass panes at the two ends of the pillar. The heat transfer per unit length of the edge increases, since the edge conduction increases with increasing glass sheet thickness. Since this rate of the increase is larger than the rate of the decrease of the heat transfer through the pillar array, the heat transfer rate through the whole glazing increases, thus the *U*-value of the whole glazing system increases.

Vacuum glazings with dimensions of 0.3 m by 0.3 m, 0.5 m by 0.5 m and 1 m by 1 m were simulated. For 2 mm, 3 mm, 4 mm, 5 mm and 6 mm thick glass panes, the values of pillar separation, pillar radius and minimal conductance of pillar array determined using the

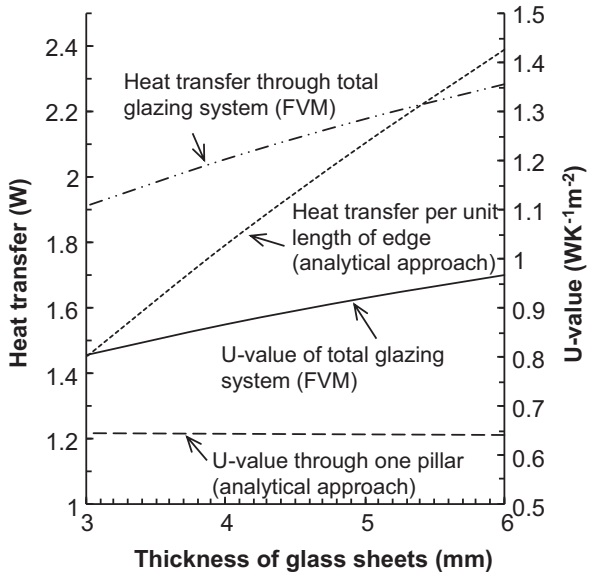

Fig. 6.2. The effect of the glass sheet thickness on the thermal performance of an evacuated glazing calculated by both an analytical approach and a finite volume model (FVM).

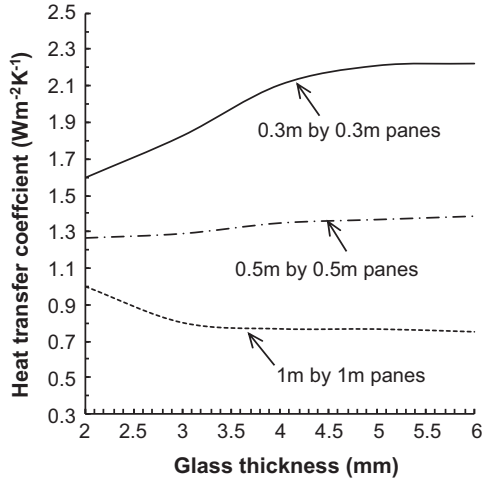

Fig. 6.3. The predicted thermal performance of an evacuated glazing with pillar separation and pillar radius specified in Table 5.1 [41].

above four restrictions and listed in Table 5.1 were used in the simulation. Using the finite volume model, the thermal performances of these glazing systems were analysed and the results are illustrated in Fig. 6.3 [41].

Fig. 6.3 shows that for the vacuum glazing systems of 0.3 m by 0.3 m and 0.5 m by 0.5 m dimensions, the thinner the glass panes are, the lower their heat transfer coefficients are. For both of these systems, increasing the glass thickness leads to an increase in their heat transfer coefficients. When the evacuated glazing size is 1 m by 1 m, increasing the glass pane thickness up to 3.5 mm leads to a decrease in the heat transfer coefficient, further increases in the glass thickness do not lead to further reduction in the heat transfer coefficient.

7. Ageing of vacuum glazing

If the level of vacuum deteriorates or the emittance of the internal low-e coatings increases, the thermal insulation will degrade. The emittance of pyrolitically deposited coatings has been found degraded slightly (by 10–15%) after being subjected to high temperature in the process of forming the edge seal [32].

The combined gaseous and radiative conductance has been measured over several years on sealed vacuum glazing samples in the USD [76]. These measurements were made in a guarded hot plate apparatus at room temperature. Within the accuracy and stability of the apparatus, there was no evidence of vacuum degradation [76]. At the UU, indium alloy based vacuum glazing samples were subjected to extreme ambient conditions within the guarded hot box [39]. Thermal cycling tests were undertaken in which the air temperature on one side of the sample was taken from −30 °C to +50 °C and back to −30 °C 15 times while maintaining an air temperature of 22 °C on the other side. After this test procedure, it was found that the glass to glass heat conductance at the centre glazing area had increased by 10.1% from which the vacuum pressure within the evacuated space was determined to have increased from the negligible level of less than 0.1 Pa to 0.16 Pa using the model of Corrucini [50]. Previous research [32,39] has shown that if the vacuum pressure is less than 0.1 Pa, the effect of conduction through the residual gas on the total glazing heat transfer is negligible. The degradation of vacuum level determined was corroborated by the change in glass surface temperatures. The experimental results showed that the samples can bear these extreme conditions.

Two different physical mechanisms of vacuum degradation within vacuum glazing have been investigated by the team at the USD. When vacuum glazing samples are stored in a high temperature environment, the evolution of water vapour can occur [82,83]. If the glazing samples are exposed to sunlight [84] or external energy excitation [85] such as a laser beam, the evolution of CO and CO_2 can happen. If vacuum glazing samples were not subjected to either sunlight or laser light, water evolution could be the cause of the measured vacuum degradation resulting after thermal cycling.

Although a complete understanding has not been obtained about the physical processes which can cause vacuum degradation, and also about the rates of such degradations, it is however possible to draw several conclusions about the stability of the vacuum under high temperature ageing.

- the rate of vacuum degradation is increased by elevating the storage temperature,
- at any given storage temperature, samples which had been baked at higher temperatures during the evacuation process exhibit a lower rate of vacuum degradation,
- the internal pressure within a degraded vacuum glazing sample was dependent on the ageing temperature; the pressure decreases as the ageing temperature is decreased. It is believed that this was due to the adsorption of the gas onto the internal surfaces of the glazing, and
- the temperature dependence of the vacuum pressure was strongly dependent on the fabrication process of the vacuum glazing (specifically dependent on the temperature and time of outgassing during the evacuation process), on the amount of the degradation of the internal vacuum, and on the type of the internal surfaces (for example K glass or uncoated glass) [32,39].

8. Development of electrochromic vacuum glazing

An electrochromic (EC) vacuum glazing (EC VG) has been developed by the Ulster group, which is the combination of an EC glazing and a vacuum glazing as shown in Fig. 8.1 [46]. This

novel glazing system combines the low-heat-loss properties of vacuum glazing with a *U*-value of less than 1 W m^{-2} K^{-1} with the variable light transmittance of EC glazing to allow control of solar heat gain. The light transmittance can be controlled between 20% in the coloured state and 80% in the bleached state by applying a 1 to 2 V DC switching voltage. The combination of these properties may provide improved thermal comfort, with limited use of auxiliary space heating and artificial light due to the very low heat loss and potential control of day lighting and glare.

An extensively validated finite volume model was modified [37] to analyse heat transfer through an EC VG for ASTM standard winter boundary conditions. One quarter pane of the EC VG was modelled to represent the full pane due to symmetric configuration of EC VG. The pillar array was incorporated and modelled directly in the finite volume model. The graded mesh with a high density of nodes in and around the pillar provided an adequate representation of the heat transfer. Simulations showed that the EC layer should face towards the outdoor environment; when the EC layer faced inwards, glazing surface temperatures would be too high for occupant comfort and would result in damage to the EC VG system.

For insolation of between 0 and 1000 W m^{-2} incident perpendicular to the glazing surface, the calculated mean surface temperatures of the outdoor and indoor glass pane surfaces are shown in Fig. 8.2.

Fig. 8.2 shows that with increasing the level of insolation incident perpendicular to the glazing surface from 0 to 1000 W m^{-2}, the rate of increase in mean surface temperatures of the outdoor glass pane is significantly larger than that of the indoor glass pane, due to the absorbed solar energy by the EC layer on the outdoor glass pane. At insolations greater than 200 W m^{-2}, the indoor glass pane due to absorbed radiation transfers heat to the indoor environment; when the insolation is greater than 370 W m^{-2}, the temperature of the outdoor glass pane is greater than that of indoor glass pane.

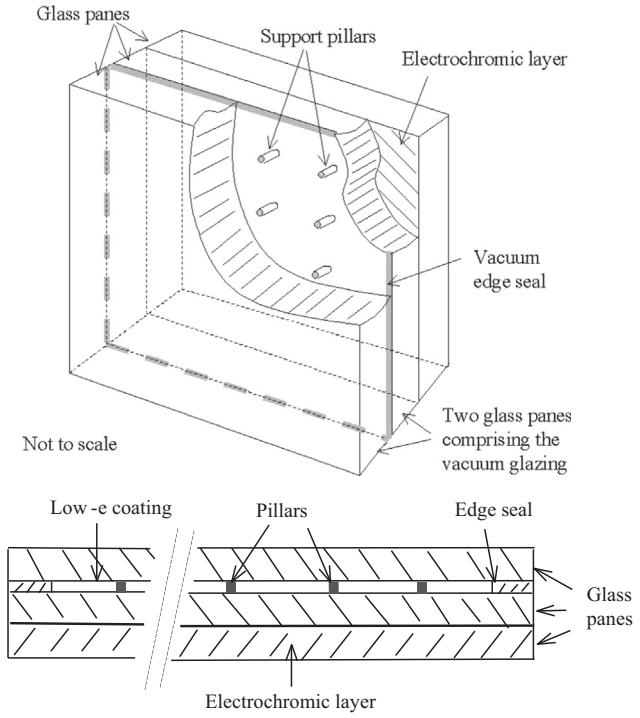

Fig. 8.1. Schematic diagram of an EC VG.

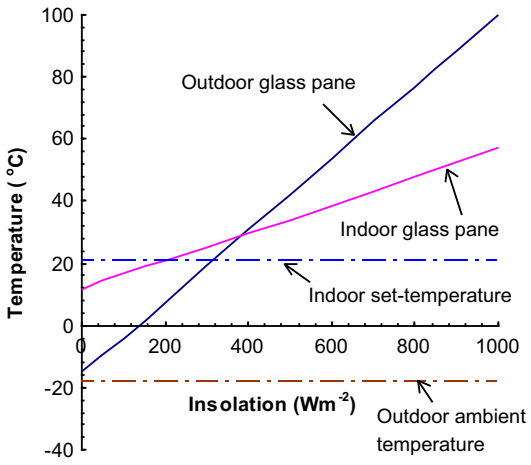

Fig. 8.2. The mean surface temperatures of the indoor and outdoor glass panes of a 0.4 m by 0.4 m EC VG under insolation incident on the outdoor glass surface between 0 and 1000 W m^{-2} [37].

9. Fabrication and characterization of indium alloy based hybrid vacuum glazing

In order to further improve the thermal performance of vacuum glazing the concept of hybrid vacuum glazing (HVG) has been introduced [71,44]. As shown in Fig. 9.1 HVG consists of a vacuum glazing unit and an extra glass pane, separated by an edge spacer sealed with polysulfide. The distance between the glass pane and the vacuum glazing might vary from 6 mm to 18 mm depending on the applications, and for further insulation the space might be filled with an inert gas, and the third glass pane might have low-e coatings. Fabrication of HVG includes two stages; in the first stage a high thermal performance vacuum glazing is fabricated and in the second stage the third glass pane is combined with the vacuum glazing.

Samples of HVG were fabricated and theoretically and experimentally characterized using a finite element model and a hot box calorimeter, respectively [44]. In the process of fabrication of the HVG, indium alloy based vacuum glazing were fabricated which comprised two 4 mm *k*-glass panes of 0.4 m × 0.4 m separated by arrays of stainless steel support pillars (0.15 mm high and 0.4 mm in diameter) spaced at 25 mm intervals. Each glass pane had a low-e coating with emittance of 0.16 on one side which faced the vacuum gap. The fabrication method of vacuum glazing

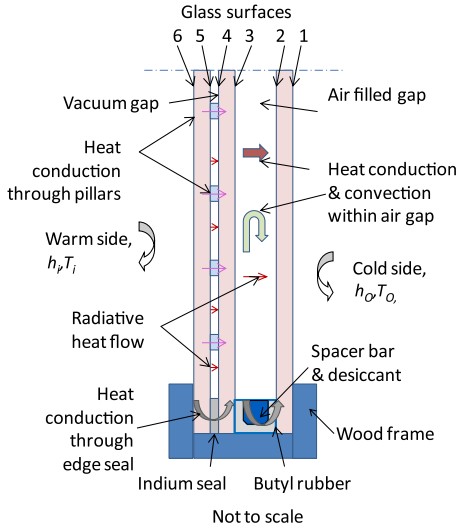

Fig. 9.1. A schematic diagram of a HVG.

is described in detail in Section 2. The samples showed good thermal performance with a *U*-value of 0.86 W m^{-2} K^{-1} and 1.10 W m^{-2} K^{-1} for the central and total glazing area, respectively. After preparing the vacuum glazing, the third glass pane (a 4 mm float glass pane) was combined to the vacuum glazing using Polysulfide as a sealant. A 12 mm wide aluminum spacer separated the third pane from the vacuum glazing, and the cavity was left air-filled. The experimental characterization of the hybrid vacuum glazing samples demonstrated excellent thermal performance with a *U*-value of 0.66 W m^{-2} K^{-1} and 0.91 W m^{-2} K^{-1} for the central and total glazing area, respectively; the experimental and theoretical results are in good agreement.

10. Fabrication and characterization of indium alloy based triple vacuum glazing

In order to further improve the thermal performance of vacuum glazing the concept of triple vacuum glazing (TVG) has been introduced [86]. Using numerical methods the thermal performance of TVG has been discussed [87,47]. TVG consists of three panes of glass joined together around the edges with a hermetic (leak-free) seal, and separated by a narrow (~0.2 mm) evacuated space as shown in Fig. 10.1 Internal arrays of tiny high strength support pillars maintain the spacing of the glass panes under the influence of atmospheric pressure. Samples of TVG were fabricated for first time using indium alloy as a sealant [88]. The three glass panes were bonded together with indium alloy using an ultrasonic soldering technique; this process is described in Section 2. After the edge seal formation and subsequent cool down of the glazing assembly, a turbo molecular vacuum pump was connected to the glazing using a pump-out cup as shown in Fig. 2.4. During the evacuation process the glass assembly was re-heated up to 150 °C for 7 h in a bake-out oven to outgas the internal glazing surfaces. The fabricated glazing comprised three 4 mm thick glass panes of 0.4 m by 0.4 m, with low-e coatings with emittance of 0.16 on one side of each glass pane which were in contact with the vacuum. The support pillars, made of stainless steel had a diameter of 0.4 mm and a height of 0.15 mm; Fig. 10.1 shows a schematic diagram of a TVG.

Total heat flow across the triple vacuum glazing was theoretically calculated using a finite volume model described in detail elsewhere [48]. The experimental characterization of the triple vacuum glazing demonstrated excellent thermal performance with a *U*-value of 0.43 W m^{-2} K^{-1} and 0.88 W m^{-2} K^{-1} for the central and total glazing areas, respectively; the experimental measurement and theoretical prediction results were in good agreement.

11. Conclusions and future work

Vacuum glazing has been fabricated using high temperature and low temperature fabrication processes, its thermal performance and durability have been experimentally tested. The high temperature fabrication method has been commercialised by Nippon glass Ltd. Heat flow through vacuum glazing occurs by different mechanisms i.e. by conduction through the support pillars, the edge seal and any residual gas, by radiation between the glass panes and by convection in any residual gas. These mechanisms have been modelled by analytic model and finite element/volume models; the predictions have been experimentally validated and found to be in excellent agreement. Vacuum behaviour within vacuum glazing is well understood. Significant stress exists across vacuum glazing due to atmospheric pressure and applied temperature differences between two sides of the glazing [89,90]; stress across vacuum glazing is not reviewed in this paper due to space limitations. Nevertheless the aging and thermal cycling work discussed here has proved that vacuum glazing developed by the two methods can survive under extreme weather conditions.

The edge seal in vacuum glazing is a thermal bridge transferring relatively large amounts of heat compared to the high insulation vacuum gap. Highly efficient complex multimaterial frames have been designed and fabricated to reduce the total heat flow through vacuum glazing by 20%; this is due to the use of highly insulating material within the frame exoskeleton. The low temperature fabrication method of vacuum glazing enables the use of soft low-e coatings and tempered glass in the construction of vacuum glazing. Soft low-e coated glass panes have been used in the construction of vacuum glazing at the UU, but the use of tempered glass is the work yet to be done. By using tempered glass, the separation of support pillars could be significantly increased, so the heat conductance through pillars would be reduced. Due to the high cost of indium alloy, development of alternative sealing materials seems to be necessary. Since solar heat gain is crucial in energy efficient buildings it is necessary to investigate such a factor in relation to vacuum glazing. Systematic research on solar heat gain through vacuum glazing units seems to be necessary in the future.

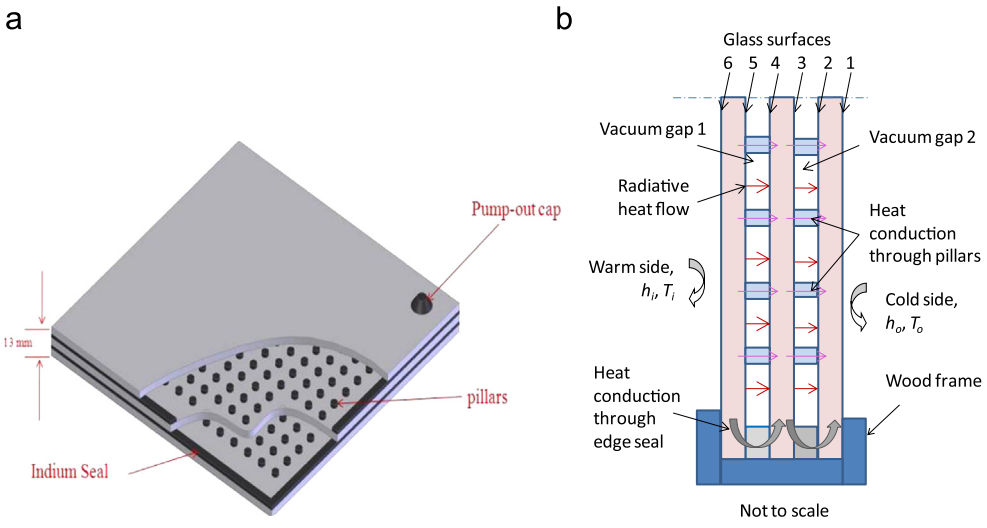

Fig. 10.1. Schematic diagrams (a) and (b) of indium alloy based TVG.

Considerable simulation work for TVG has been done [43,47,48,87]. A minimum *U*-value has been predicted down to about 0.2 W m^{-2} K^{-1} when using two vacuum gaps. There are still many challenges such as creating double edge seals in the construction of TVG, it can be hoped that any obstacles will be overcome in the near future. Electrochromic vacuum glazing which comprises a normal double vacuum glazing and the third glass pane with electrochromic coating has been developed [46,37], which can provide improved thermal comfort for occupants and reduce heating loads in winter and cooling loads in summer. Field tests for this product are necessary. Vacuum glazing could have applications in refrigerators and flat plate solar heat collectors.

Acknowledgement

The authors acknowledge the support from the EU (No: ENK6-CT-2001-00547) EPSRC (No: GR/S08251/01) of UK and Charles Parson Energy Research Awards (No: 9331 V1203) of the Department of Communications, Marine and Natural Resources, Ireland.

References

[1] Zoller F. Hollow pane of glass. German patent 387655; 1924.
[2] Kirlin I.M. Insulating pane. US patent 1370974; 1921.
[3] Chalons F.R. Transparent insulating panel. French patent 2294315; 1976.
[4] Falbel G. Evacuated dual glazing system. US patent 3990201; 1976.
[5] Rowe. Insulating materials. US patent 3936553; 1976.
[6] Hermann W., Horster H. Evacuated thermal insulating glazing unit with an infrared reflecting coating. US patent 4038797; 1977.
[7] Kesslring F. Thermally insulating window. Swiss patent 588008; 1977.
[8] Bennett C.J. Flat vacuum container. German patent 2755013; 1978.
[9] Kenney N.S. Vacuum window for solar transmission. US patent 4186723; 1980.
[10] Bourdel J. Transparent insulating panes. French patent 2483564; 1981.
[11] Ivorra C. Method of joining two transparent panes. French patent 2526066; 1983.
[12] Kreisman W.S. Method of fabricating a thermal pane window and product. US patent 4393105; 1983.
[13] Assarsson T. Heat-insulating glass. European patent 0047725; 1985.
[14] Benson D.K., Tracy C.E. Laser sealed vacuum insulation window. US patent 4683154; 1987.
[15] Viert K.P. Multiple insulating glazing with a high vacuum and supports between the sheets. German patent 3615179A1; 1987.
[16] Beuther P.D. Evacuated dual pane window structure. US patent 4786344; 1988.
[17] Collins R.E., Robinson S.J. A thermally insulating glass panel and method of construction. Patent application PCT/AU90/00364; 1990.
[18] Demars Y., Mullar R. Method to produce a vacuum in an insulating glazing and an insulating glazing. European patent 0645516AZ; 1995.
[19] Parker K.R. Insulating glazing unit. Canadian patent 1290624; 1991.
[20] Bachli E. Thermally insulating construction and/or lighting element. US patent 5009218; 1991.
[21] Bachli E. Gastight edge seal. European patent 0434802B1; 1992.
[22] Kerr T.P., Liu S.B., Harmon P.P., Siskos W.R., Oravitz J.J.L., Shaffer P.E. Vacuum insulating unit. US patent 5124185; 1992.
[23] Collins RE, Robinson SJ. Evacuated glazing. Sol Energy 1991;47:27–38.
[24] Griffiths PW, Di Leo M, Cartwright P, Eames PC, Yianoulis P, Leftheriotis G, et al. Fabrication of evacuated glazing at low temperature. Sol Energy 1998;63(4):243–9.
[25] Griffiths PW, Eames PC, Hyde TJ, Fang Y, Norton B. Experimental characterization and detailed performance prediction of a vacuum glazing system fabricated with a low temperature metal edge seal, using a validated computer model. J Sol Energy Eng Trans ASME 2006;128(2):199–203.
[26] Hyde T.J., Griffiths P.W., Eames P.C., Norton B. Development of a novel low temperature edge seal for evacuated glazing. In: Proceeding of world renewable energy congress VI (WREC2000). Brighton, UK; 2000. p. 271–74.
[27] Zhao JF, Eames PC, Hyde TJ, Fang Y, Wang J. A modified pump-out technique used for fabrication of low temperature metal sealed vacuum glazing. Sol Energy 2007;81(9):1072–7.
[28] Benson D.K., Tracy C.E., Jorgensen G.J. Laser sealed evacuated window glazings. In: 28th SPIE int. symp. on optics and electro-optics. San Diego, CA; 1984;.
[29] Benson D.K., Tracy C.E. Evacuated window glazings for energy efficient buildings. In: 29th SPIE int. symp. on optics and electro-optics. San Diego, CA; 1985.
[30] Benson D.K., Tracy C.E. Vacuum window glazings for energy efficient buildings. Internal report PR-2901, Solar Energy Research Institute, 1986, Golden, CO.
[31] Robinson SJ, Collins RE. Evacuated windows—theory and practice. In: Proceeding of ISES solar world congress; 1989; Kobe, Japan. Oxford: Pergamon; 1989.
[32] Collins RE, Simko TM. Current status of the science and technology of vacuum glazing. Sol Energy 1998;62:189–213.
[33] Pilkington datasheet. ⟨http://www.pilkington.com/products/bp/bybenefit/thermalinsulation/kglass⟩ (accessed August 4, 2013).
[34] Fang Y, Eames PC, Hyde TJ, Norton B. Complex multimaterial insulating frames for windows with evacuated glazing. Sol Energy 2005;79(3):245–61.
[35] Fang Y, Eames PC, Norton B, Hyde TJ. Experimental validation of a numerical model for heat transfer in vacuum glazing. Sol Energy 2006;80(5):564–77.
[36] Fang Y, Eames PC. The effect of glass coating emittance and frame rebate on heat transfer through vacuum and electrochromic vacuum glazed windows. Sol Energy Mater Sol Cells 2006;90(16):2683–95.
[37] Fang Y, Eames PC. Thermal performance of an electrochromic vacuum glazing. Energy Convers Manage 2006;47(20):3602–10.
[38] Fang Y., Eames P.C., Norton B., Hyde J.T., Hewitt N. The influence of edge seal and size on the thermal performance of evacuated glazing. In: Proceeding of the heat—SET 2007 conference. April 18–20; Chambery, France; 2007. p. 969–74. isbn:2-9502555-4-X.
[39] Fang Y, Hyde T, Eames PC, Hewitt N. Theoretical and experimental analysis of the vacuum pressure in a vacuum glazing after extreme thermal cycling. Sol Energy 2009;83(9):1723–30.
[40] Fang Y, Hyde T, Hewitt N, Eames PC, Norton B. Comparison of vacuum glazing thermal performance predicted using two- and three-dimensional models and their experimental validation. Sol Energy Mater Sol Cells 2009;93(9):1492–8.
[41] Fang Y, Eames PC, Norton B. Effect of glass thickness on the thermal performance of evacuated glazing. Sol Energy 2007;81(3):395–404.
[42] Fang Y, Eames PC, Norton B, Hyde TJ, Zhao J, Wang J, et al. Low emittance coatings and the thermal performance of vacuum glazing. Sol Energy 2007;81(1):8–12.
[43] Fang Y., Hyde T.J., Hewitt N. The effect of insolation on the thermal performance of triple vacuum glazing. In: Proceeding of glass performance days (GPD) conference. June 17–20; Tampere, Finland; 2011 p. 57–60.
[44] Fang Y, Hyde T, Arya F, Hewitt N. A novel building component hybrid vacuum glazing - a modelling and experimental validation. ASHRAE Trans 2013;119(2):403–41.
[45] Fang Y. An experimental and theoretical investigation into the design, development and performance of evacuated glazing. PhD thesis. Jordanstown, UK: University of Ulster; 2003.
[46] Fang Y, Hyde T, Hewitt N, Eames PC, Norton B. Thermal performance analysis of an electrochromic vacuum glazing with low emittance coatings. Sol Energy 2010;84(4):516–25.
[47] Fang Y, Hyde TJ, Hewitt N. Predicted thermal performance of triple vacuum glazing. Sol Energy 2010;84(12):2132–9.
[48] Fang Y., Hyde T.J., Hewitt N. The influence of emittance of low-emittance coating on the thermal performance of triple vacuum glazing. In: Proceedings of the second IASTED international conference on solar energy, SOE 2010. July 15–17; Banff, Alberta, Canada; 2010. p. 921–28. Available in CD, isbn:978-0-88986-843-4.
[49] Garrison JD, Collins RE. Manufacture and cost of vacuum glazing. Sol Energy 1995;55(3):151–61.
[50] Corrucini RJ. Gaseous heat conduction at low pressures and temperatures. Vacuum 1957;7–8:19–29.
[51] Friedl W. USB UtraSonic Bond—divetailing flat glass and metal as an alternative to glue, drill and screw. In: Proceeding of glass performance days (GPD) conference. June 17–20; Tampere, Finland; 2011. p. 299–300.
[52] Bettger K., Stark D.H. Flexible edge seal for vacuum insulating glazing units. US patent 20100178439; 2010.
[53] Simko T.M. Heat transfer processes and stresses in vacuum glazing. PhD thesis. Sydney, Australia: University of Sydney; 1996.
[54] Griffiths PW, Norton B, Eames PC, Lo SNG. Detailed simulation of heat transfer across planar evacuated glazing: In this paper techniques are described for modelling heat flow through evacuated glazing. Modelling results are compared with infra-red thermography. Build Res Inf 1996;24(3):141–7.
[55] Simko T.M., Collins R.E., Beck F.A., Arasteh D. Edge conduction in vacuum glazing. Paper presented at: ASHRAE/DOE thermal performance of the exterior envelopes of buildings VI conference. Dec 4–8; 1995.
[56] Glass in building—determination of luminous and solar characteristics of glazing, EN410. April; 1998.
[57] Johnson TE. Low-e glazing design guide. Boston: Butterworth-Heinemann; 1991.
[58] Duffie JA, Backman WA. Solar engineering of thermal process. New York, NY: John Wiley and Son; 1991.
[59] Griffiths P.W. An examination of the thermophysical nature of solar control films using an illuminated hot box and computer based simulation modelling techniques. PhD thesis. Cranfield; 1995.
[60] Leftheriotis G, Yianoulis P, Patrikios D. Deposition and optical properties of optimised ZnS/Ag/ZnS thin films for energy saving applications. Thin Solid Films 1997;306(1):92–9.
[61] Leftheriotis G, Yianoulis P. Characterization and stability of low-emittance multiple coatings for glazing applications. Sol Energy Mater Sol Cells 1999;58(2):185–97.
[62] Leftheriotis G, Papaefthimiou S, Yianoulis P. Integrated low-emittance-electrochromic devices incorporating ZnS/Ag/ZnS coatings as transparent conductors. Sol Energy Mater Sol Cells 2000;61(2):107–12.
[63] Zhang Q-C, Simko TM, Dey CJ, Collins RE, Turner GM, Brunotte M, et al. The measurement and calculation of radiative heat transfer between uncoated and

doped tin oxide coated glass surfaces. Int J Heat Mass Transfer 1996;40 (1):61–71.
[64] Dixon J.R. Chapter 3: electric-susceptibility mass of free carriers in semiconductors. In: Nudelman S, Mitra SS, editors. Optical properties of solids; 1996.
[65] A PC program WINDOW 6.0 for analysing window thermal performance. Lawrence Berkeley Laboratory Berkeley, CA94720. 2010.
[66] Wilson CF, Simko TM, Collins RE. Heat conduction through the support pillars in vacuum glazing. Sol Energy 1998;63(6):393–406.
[67] Collins RE, Fischer-Cripps AC. Design of pillar arrays in flat evacuated windows. Aust J Phys 1991;44:73–86.
[68] Fischer-Cripps AC, Collins RE. The probability of hertzian fracture. J Mater Sci 1994;29(8):2216–30.
[69] Griffiths P.W., Eames P.C., Hyde T.J., Norton B. A low temperature sealed vacuum glazing system, performance, analysis and predicted economic and environmental benefits. In: Proceeding of world renewable energy congress VI (WREC2000). Brighton, UK; 2000. p. 207–12.
[70] Standard procedures for determining the steady state thermal transmittance of fenestration systems, ASTM standard; 1991. p. E1423–91.
[71] Collins R.E., AsAno O., Misonou M., Katoh H., Nagasaka S. Vacuum glazing: design options and performance capability. In: Paper presented at: glass in buildings conference. Bath, UK; 1999.
[72] Collins RE, Davis CA, Dey CJ, Robinson SJ, Tang J-Z, Turner GM. Measurement of local heat flow in flat evacuated glazing. Int J Heat Mass Transfer 1993;36: 2553–63.
[73] Eames PC, Norton B. Validated, unified model for optics and heat transfer in line-axis concentrating solar energy collectors. Sol Energy 1993;50(4):339–55.
[74] Griffiths P.W., Eames P.C., Norton B. Thermal properties of evacuated glazing based on experimental solar simulation and computer based simulation modelling. In: Ledbetter S, Harris R, editors. Proceedings of international conference on building envelop systems technology. April; Bath, UK; 1997. p. 343–48.
[75] Mushfegh B, Lloyd D, Karlsson B. Heat transfer at modern windows—rish of condensation. Energy Build 1989;13:119–25.
[76] Collins RE, Turner GM, Fischer-Cripps AC, Tang JZ, Simko TM, Dey CJ, Clugston DA, Zhang QC, Garrison JD. Vacuum glazing—a new component for insulating windows. Build Environ 1995;30(4):459–92.
[77] Springer GS. Heat transfer in rarefied gases. In: Irvine F, Hartnett JP, editors. Advances in heat transfer. New York, NY: Academic Press; 1971. p. 163–218.
[78] Elmahdy AH. Heat transmission and *R*-value of fenestration systems using IRC hot box: procedure and uncertainty analysis. ASHRAE Trans 1992;98:630–7.
[79] Simko TM, Elmahdy AH, Collins RE. Determination of the overall heat transmission coefficient (*U* value) of vacuum glazing. ASHRAE Trans 1999;105: 891–9.
[80] Wendt JF. Computational fluid dynamics. Berlin Heidelberg: Springer-Verlag; 1996.
[81] Holman JP. Heat transfer (SI metric ed.). McGraw-Hill; 1989.
[82] Lenzen M, Turner GM, Collins RE. Thermal outgassing of vacuum glazing. J Vac Sci Technol A: Vac Surf Films 1999;17(3):1002–17.
[83] Ng N, Collins RE, So L. Thermal and optical evolution of gas in vacuum glazing. Mater Sci Eng B: Solid-State Mater Adv Technol 2005;119(3):258–64.
[84] Ng N, Collins RE, So L. Photodesorption of gases in vacuum glazing. J Vac Sci Technol A: Vac Surf Films 2003;21(5):1776–83.
[85] Minaai T, Kumagai M, Nara A, Tanemura S. Study of the outgassing behavior of SnO_2:F films on glass in vacuum under external energy excitation. Mater Sci Eng B: Solid-State Mater Adv Technol 2005;119(3):252–7.
[86] Wuethrich W. Heat transmission reducing closure element. European patent 152992; 2005.
[87] Manz H, Brunner S, Wullschleger L. Triple vacuum glazing: Heat transfer and basic mechanical design constraints. Sol Energy 2006;80(12):1632–42.
[88] Arya F., Fang Y., Hyde T. Fabrication and characterization of triple vacuum glazing at low temperature using an indium-based seal. In: Paper presented at: the energy and material research conference EMR; 2012 June; Malaga, Spain. Florida: Brown Walker Press; 2012. p. 521–524.
[89] Wang J, Eames PC, Zhao JF, Hyde T, Fang Y. Stresses in vacuum glazing fabricated at low temperature. Sol Energy Mater Sol Cells 2007;91(4):290–303.
[90] Wullschleger L, Manz H, Ghazi Wakili K. Finite element analysis of temperature-induced deflection of vacuum glazing. Constr Build Mater 2009;23(3):1378–88.